

Washington University in St. Louis

## Washington University Open Scholarship

---

All Theses and Dissertations (ETDs)

---

5-24-2012

### Propulsion By Sinusoidal Locomotion: A Motion Inspired By Caenorhabditis Elegans

Xialing Ulrich

*Washington University in St. Louis*

Follow this and additional works at: <https://openscholarship.wustl.edu/etd>

---

#### Recommended Citation

Ulrich, Xialing, "Propulsion By Sinusoidal Locomotion: A Motion Inspired By Caenorhabditis Elegans" (2012). *All Theses and Dissertations (ETDs)*. 731.

<https://openscholarship.wustl.edu/etd/731>

This Dissertation is brought to you for free and open access by Washington University Open Scholarship. It has been accepted for inclusion in All Theses and Dissertations (ETDs) by an authorized administrator of Washington University Open Scholarship. For more information, please contact [digital@wumail.wustl.edu](mailto:digital@wumail.wustl.edu).

WASHINGTON UNIVERSITY IN ST. LOUIS  
School of Engineering and Applied Science  
Department of Mechanical Engineering and Material Science

Thesis Examination Committee:

Dr. David Peters  
Dr. Philip Bayly  
Dr. William Pickard  
Dr. Guy Genin  
Dr. Norman Katz

PROPULSION BY SINUSOIDAL LOCOMOTION: A MOTION INSPIRED BY

*CAENORHABDITIS ELEGANS*

by

Xialing Ulrich

A dissertation presented to the School of Engineering  
of Washington University in partial fulfillment of the  
requirements for the degree of

DOCTOR OF SCIENCE

May 2012  
Saint Louis, Missouri

copyright by  
Xialing Ulrich  
2012

## ABSTRACT OF THE THESIS

Propulsion by Sinusoidal Locomotion: a Motion Inspired by *Caenorhabditis elegans*

by

Xialing Ulrich

Doctor of Science in Mechanical Engineering

Washington University in St. Louis, 2012

Research Advisor: Professor David Peters

Sinusoidal locomotion is commonly seen in snakes, fish, nematodes, or even the wings of some birds and insects. This doctoral thesis presents the study of sinusoidal locomotion of the nematode *C. elegans* in experiments and the application of the state-space airloads theory to the theoretical forces of sinusoidal motion. An original MATLAB program has been developed to analyze the video records of *C. elegans*' movement in different fluids, including Newtonian and non-Newtonian fluids. The experimental and numerical studies of swimming *C. elegans* has revealed three conclusions. First, though the amplitude and wavelength are varying with time, the motion of swimming *C. elegans* can still be viewed as sinusoidal locomotion with slips. The average normalized wavelength is a conserved character of the locomotion for both Newtonian and non-Newtonian fluids. Second, fluid viscosity affects the frequency but not the moving speed of *C. elegans*, while fluid elasticity affects the moving speed but not the frequency. Third, by the resistive force theory, for more elastic fluids the ratio of resistive coefficients  $K = C_n/C_l$  becomes smaller.

Inspired by the motion of *C. elegans* and other animals performing sinusoidal motion, we investigated the sinusoidal motion of a thin flexible wing in theory. Given the equation of the motion, we have derived the closed forms of propulsive force, lift and other generalized forces applying on the wing. We also calculated the power required to perform the motion, the power lost due to the shed vortices and the propulsive efficiency. These forces and powers are given as functions of reduced frequency  $k$ , dimensionless wavelength  $z$ , dimensionless amplitude  $A/b$ , and time. Our results show that a positive, time-averaged propulsive force is produced for all  $k > k_0 = \pi/z$ . At  $k = k_0$ , which implies the moment when the moving speed of the wing is the same as the wave speed of its undulation, the motion reaches a steady state with all forces being zero. If there were no shed vorticity effects, the propulsive force would be zero at  $z = 0.569$  and  $z = 1.3$  for all  $k$ , and for a fixed  $k$  the wing would gain the optimal propulsive force when  $z = 0.82$ . With the effects of shed vorticity, the propulsive efficiency decreases from 1.0 to 0.5 as  $k$  goes to infinity, and the propulsive efficiency increases almost in a linear relationship with  $k_0$ .

# Acknowledgments

There are many people to whom I would like to convey my gratitude. Many thanks to my current advisor, Professor David Peters, whose theory of flexible airfoils is the background of the theoretical part of my research, and these results are the highlights of this dissertation. I am also very thankful to Professor Amy Shen, my former advisor, who guided me in starting my research in *C.elegans* and fully supported the experimental part of this thesis. I am very grateful to Professor William Pickard, who offered me his own lab space for the past four years and has been mentoring and encouraging me to pursue the doctoral degree even when it seemed impossible. Much appreciation to Professor Guy Genin, in that it was his suggestion to apply professor Peters' theory to my experiments. I would like to thank Professor Michael Nonet from the School of Medicine for his generous and continuous provision of *C. elegans* for all my experiments.

Many appreciations to my dear husband Bob for his fellowship and whole-hearted support, to my parents who have been traveling between the US and China many many times to help take care of my little children, and to my two precious children, Noah and Abigail, who bring me a lot of love and joy.

Xialing Ulrich

*Washington University in Saint Louis*  
*May 2012*

Dedicated to my family.

# Contents

Abstract . . . . .	ii
Acknowledgments . . . . .	iv
List of Tables . . . . .	viii
List of Figures . . . . .	ix
Nomenclature . . . . .	xii
<b>1 Introduction . . . . .</b>	<b>1</b>
1.1 Sinusoidal Locomotion . . . . .	1
1.2 Governing Equations . . . . .	3
1.3 The State-Space Airloads Theory . . . . .	5
<b>2 Sinusoidal Locomotion of <i>C. elegans</i> . . . . .</b>	<b>9</b>
2.1 Experimental Setup and Procedure . . . . .	9
2.2 Data Analysis . . . . .	12
2.3 Results . . . . .	15
2.3.1 The locomotory gaits of <i>C. elegans</i> . . . . .	15
2.3.2 Statistical results and viscoelastic effects . . . . .	18
2.3.3 Resistive coefficients of viscoelastic fluids . . . . .	21
<b>3 Propulsion by Sinusoidal Locomotion at High Reynolds Numbers</b>	<b>23</b>
3.1 Coordinate System and Equation of Sinusoidal Motions . . . . .	23
3.2 Propulsion, Lift and Generalized Forces . . . . .	25
3.2.1 Case of no shed vorticity . . . . .	27
3.2.2 Shed vorticity effects . . . . .	28
3.2.3 Time-averaged propulsion . . . . .	30
3.3 Propulsive Efficiency . . . . .	31
3.4 Numerical Results . . . . .	34
3.5 Summary . . . . .	42
<b>4 Discussion . . . . .</b>	<b>44</b>
<b>5 Conclusions . . . . .</b>	<b>46</b>



Appendix A	Proofs of Certain Identities Involving Bessel Functions	48
References	.....	52
Vita	.....	54

# List of Tables

2.1	Zero shear viscosity and relaxation time of the testing fluids. . . . .	12
2.2	Statistical results of the locomotory data. # is the number of samples studied. The results are given as the average $\pm$ the standard deviation.	19

# List of Figures

1.1	Sinusoidal locomotion seen in nature. The dimensions of these animals are varying from 1 mm to 5 m. . . . .	2
1.2	A general moving coordinate system for the state-space airloads theory. . .	5
2.1	The experiment setup and procedure. A featureless device made of a rubber O-ring and a cover glass was used as the observation station of swimming <i>C. elegans</i> . A microscope camera was used to record the motion and the movies were analyzed by a MATLAB program. . . . .	10
2.2	The user interface of the MATLAB image processing and data analysis program. . . . .	13
2.3	The procedure of image processing and data analysis. 1) A sequence of sinusoidal locomotion over one period is manually selected. Sample shown is from <i>C. elegans</i> in 5PVP. 2) After image processing, the coordinates of 11 body points (dots) are found for each frame. The first and last frame of the sequence are overlaid to find the moving direction and other important parameters. 3) Tracks of body points are used to find the amplitudes $A(i)$ . . . . .	15
2.4	The body length, normalized amplitude, and normalized wavelength of <i>C. elegans</i> in 5PVP, 10PVP, 10PVP-1000XG, and 10PVP-3000XG. Only one sample is shown for each testing fluid. The data from crawling <i>C. elegans</i> (the last column on the right) are shown to compare with the swimming gaits. . . . .	16
2.5	A comparison between the experimental data and computed data by Eqs. (2.1-2.3). The computed data is base on amplitude of 0.17, wavelength of 0.88, and moving speed 0.25 (the statistic results in 5PVP shown in Table 2.2). The contours of $v_y(s, t)$ show the locomotory gaits of <i>C. elegans</i> is sinusoidal with consistent wavelength within the experimental errors. . . . .	18
2.6	Normalized wavelength $\Lambda/L$ and normalized wavelength $A/L$ vs. zero shear viscosity $\eta_0$ and Deborah number De. Triangles indicate Newtonian fluid (5PVP in this study), squares are Boger fluids (8PVP and 10PVP ), and circles are viscoelastic fluids (all xanthan gum-PVP solutions). The error bars shows the standard deviations. . . . .	20
2.7	Frequency $f$ and moving speed $V_m/L$ vs. zero shear viscosity $\eta_0$ and De number. Relations of $f-\eta_0$ and $V_m$ -De are shown to fit the experimental data. Triangles indicate the Newtonian fluids, squares are Boger fluids and circles are viscoelastic fluids. . . . .	20

2.8	$1/\gamma$ vs. $1/B^2$ . The markers (triangle, squares and circles) are the means of the experimental data for each testing fluid. The values of De number is indicated by the color. The solid line are the theoretical prediction by the resistive force theory with different $K$ values. The slop of the lines is given by $2/(K - 1)$ and the constant is $K/(K - 1)$ . . . . .	22
3.1	A 2D coordinate system of a flexible wing performing sinusoidal locomotion. $v_0$ and $v_1$ are zeros here. . . . .	24
3.2	Numerical approximation of $M(k)$ and $N(k)$ verse scaled reduced frequency $k/(k + 1)$ . The value of $M - M^2 - N^2$ , which is a factor in lost power $\overline{C_W}$ , is also shown. . . . .	29
3.3	The time-dependent coefficients of all forces (with and without shed vorticity effects) for one undulatory period $T$ , at $A/b = 0.2$ and $z = 0.6$ and four different reduced frequencies. . . . .	34
3.4	The time-dependent coefficients of all forces (with and without shed vorticity effects) for one undulatory period $T$ , at $A/b = 0.2$ and $z = 0.9$ and four different reduced frequencies. . . . .	35
3.5	The time-dependent coefficients of all forces (with and without shed vorticity effects) for one undulatory period $T$ , at $A/b = 0.2$ and $k = 21.5$ and four different wavelength $z$ . At $z = 0.569$ and $z = 1.3$ , $\beta_0 = 0$ . At $z = 0.82$ , $\alpha_1 = 0$ and $\beta_0$ is at its region extrema. . . . .	36
3.6	Normalized time-averaged propulsive coefficient (with and without shed wake) versus scaled reduced frequency $k/(k + 1)$ at $A/b = 0.2$ and $z = 0.6$ ( $k_0/(k_0 + 1) \approx 0.84$ ). The right plot is an enlarged view of the circle in the left plot. . . . .	37
3.7	Normalized time-averaged propulsive coefficient (with and without shed wake) versus scaled reduced frequency $k/(k + 1)$ at $A/b = 0.2$ and $z = 0.9$ ( $k_0/(k_0 + 1) \approx 0.78$ ). The right plot is an enlarged view of the circle in the left plot. . . . .	38
3.8	The time-averaged propulsive coefficient (with and without shed wake) versus critical reduced frequency $k_0 = \pi/z$ at $A/b = 0.2$ . The left plot is at $k = 21.36$ , and the right one is at $k = 13.35$ . The peaks of time averaged propulsion only depend on $k_0$ (or $z$ ). . . . .	39
3.9	Time-averaged power coefficients normalized to $k(k + 1)$ versus $k/(k + 1)$ , at $A/b = 0.2$ and $z = 0.9$ (or $k_0 = 3.49$ ). $\overline{C_P}$ is the power required for wing motion, $\overline{C_F}$ is propulsive power with wake effects, and $\overline{C_W}$ is the lost power due to wake. The plot on the right is an enlarged view of the circle in the left plot. . . . .	40
3.10	The time-averaged power coefficients verse critical reduced frequency $k_0$ , for $A/b = 0.2$ , $k = 13.36$ . $\overline{C_P}$ is the power required for wing motion, $\overline{C_F}$ is propulsive power with wake effects, and $\overline{C_W}$ is the lost power due to wake. . . . .	40

3.11	The propulsive efficiency $\epsilon$ verse $(k - k_0)/(k + k_0)$ (left) and $k_0$ (right).The left plot only shows when $k > k_0$ , that is $(k - k_0)/(k + k_0) > 0$ for $A/b = 0.2$ and $z = 0.9$ . The right plot shows the results for $k = 11.78$ . . . . .	41
4.1	Both the state-space airloads theory and the experiments show back slips of sinusoidal locomotion over one period under certain condition. Blue arrows point out the negative propulsive force and slips. . . . .	45

# Nomenclature

$A$	amplitude, m
$b$	semi-chord, m
$C(k)$	Theodorsen Function
$C_F$	coefficient of propulsive force or propulsive power, $C_F = -D/(2\pi\rho bu_0^2)$
$C_l$	longitudinal resistive force coefficient
$C_L$	lift coefficient, $C_L = L_0/(2\pi\rho bu_0^2)$
$C_{L1}$	coefficient of pitching moment, $C_{L1} = L_1/(2\pi\rho bu_0^2)$
$C_{L2}$	coefficient of bending moment, $C_{L2} = L_2/(2\pi\rho bu_0^2)$
$C_n$	normal resistive force coefficient
$C_P$	coefficient of the power required for wing motion, $C_P = P/(2\pi\rho bu_0^3)$
$C_W$	coefficient of the power lost due to wake
$d$	the width of a slender body, m
$D$	drag per unit span, N/m
De	Deborah number, $De = \tau_r f$
$f$	frequency, Hz
$F$	propulsive force, N
$f_l$	resistive force longitudinal to the body per unit length, N/m
$f_n$	resistive force normal to the body per unit length, N/m
$h(x, t)$	motion of a flexible wing, down is positive, m
$h_n(x, t)$	components of $h(x, t)$ in Chebyshev polynomials, m
$i$	imaginary unit
$Im[ ]$	the imaginary part of a complex number
$J_n$	Bessel functions of the first kind
$k$	reduced frequency, $k = 2\omega b/u_0$
$k_0$	critical reduced frequency, $k_0 = \pi/z$
$K$	ratio of coefficients of resistance, $C_N/C_L$
$L$	the characteristic length, m

$L_0$	lift per unit span, N/m
$L_n$	generalized forces per unit span, N
$M$	the real part of $1 - C(k)$
$N$	the imaginary part of $1 - C(k)$
$P$	power exerted per unit span to move the wing, N/s
Re	Reynolds number
$Re[ ]$	the real part of a complex number
$s$	body coordinate along the centerline of a slender body
$S$	span length, m
St	Strouhal number, $St = 2fA/V_m$
$t$	time, s
$t_0$	initial time of observation, s
$T$	the characteristic time, s
$u_0$	$x$ -velocity of flow relative to the $x$ -axis, m/s
$U$	the characteristic speed, m/s
$v_0$	$y$ -velocity of flow relative to the $x$ -axis, m/s
$v_1$	velocity gradient, m/s
$v_l$	velocity longitudinal to the body, m/s
$v_n$	velocity normal to the body, m/s
$\bar{v}$	velocity vector, m/s
$\hat{v}$	reduced velocity due to bound vorticity, m/s
$V_m$	moving speed, m/s
$V_w$	wave speed, m/s
$w$	total induced flow, m/s
$w_n$	components of total velocity field, m/s
$(x, y)$	Cartesian coordinates of the moving system, m
$X$	normalized reduced frequency, $X = k/(k + 1)$
$z$	dimensionless wavelength, $z = \Lambda/(2b)$
$\alpha_n$	cosine factor of $h_n/b$
$\beta_n$	sine factor of $h_n/b$
$\epsilon$	total power efficiency
$\Gamma$	total bound circulation, $m^2/s$
$\Lambda$	wavelength, m

$\lambda_0$	the velocity due to shed vorticity, m/s
$\lambda_\alpha$	cosine factor of $\lambda_0/u_0$
$\lambda_\beta$	sine factor of $\lambda_0/u_0$
$\mu$	dynamic viscosity, Pa·s
$\rho$	density of surrounding fluid or air, kg/m <sup>3</sup>
$\varphi$	Glauert variable, rad
$\tau$	reduced time, $\tau = u_0 t/b$
$\tau_r$	relaxation time, s
$\omega$	angular frequency, $\omega = 2\pi f$ , rad/s
$\bar{()}$	vectors
$()^*$	dimensionless variables
$(\dot{()})$	$\partial()/\partial t$
$(\ddot{()})$	$\partial^2()/\partial t^2$
$(\dot{()})'$	$\partial()/\partial \tau$
$(\ddot{()})''$	$\partial^2()/\partial \tau^2$



# Chapter 1

## Introduction

### 1.1 Sinusoidal Locomotion

Sinusoidal undulatory locomotion is widely used by gliding and swimming animals, such as nematodes, snakes, and some slender fish [10, 14, 22]. These animals usually have slender bodies. As they are moving towards one direction, sinusoidal waves are generated and passing along the body in the opposite direction. Sinusoidal locomotion is also seen in the motion of wings of birds and insects. These wings are flexible and performing some kind of sinusoidal motion. For example, the wings of honeybees do not move up and down stiffly but rotate and reverse while flapping [2]. The size of animals that are using sinusoidal locomotion varies from a few micrometers to a few meters, and the media they are going through can be sand, water or air. Although some of these animals have legs or fins, the propulsion by sinusoidal locomotion is significant. With different undulating frequencies and wavelengths, animals are able to gain enough propulsion to drive themselves to their destinations in all kinds of environments. However, it has not been revealed how much force can be generated by these harmonic motions.

The first part of this dissertation (Chapter 2) is the experimental and numerical studies of the locomotion of *Caenorhabditis elegans* (*C. elegans*), which is typically considered to be sinusoidal locomotion [6, 10]. *C. elegans* is a free-living nematode of 1 mm in length [19]. Due to the simplicity of its body structure, which has less than 1000 cells total, *C. elegans* is one of the most popular biological models. Its cylindrical body with tapered ends but no legs or fins makes it a simple enough model

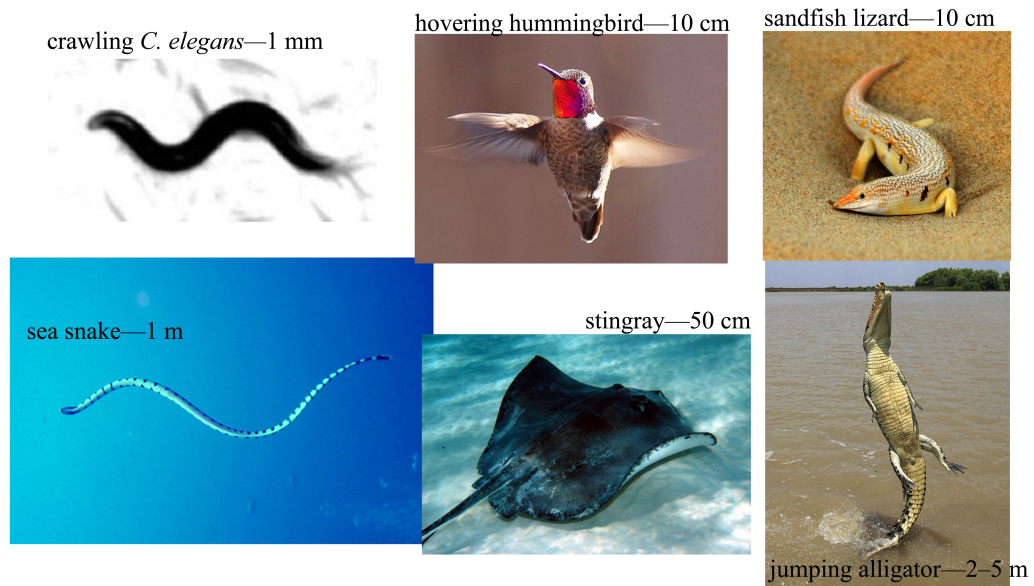


Figure 1.1: Sinusoidal locomotion seen in nature. The dimensions of these animals are varying from 1 mm to 5 m.

to study sinusoidal locomotion experimentally. The motion of *C. elegans* in a few different fluids have been recorded by a microscope video camera at a rate of 16 frames per second. When completely immersed in a fluid, *C. elegans* usually undulates on a horizontal plane and moves in a direction which is also in that plane. For this reason, its locomotion is studied in two dimensions in this dissertation. The movie clips of each undulation period are analyzed by an original MATLAB program. This program automatically captures the worm from an uniform background and finds the coordinates of its body centerline for each frame of the clip. The wavelength, frequency, amplitude, moving speed and other parameters of the locomotion are calculated from the coordinates of the body centerline. The statistic results are compared on the basis of fluid viscosity and elasticity. A kinetic equation of sinusoidal locomotion is found to match the statistical results of experiments.

## 1.2 Governing Equations

The governing equations of incompressible flow of Newtonian fluids are known as the conservation of mass plus the Navier-Stokes equations.

$$\nabla \cdot \bar{v} = 0 , \quad (1.1)$$

$$\rho \left( \frac{\partial \bar{v}}{\partial t} + \bar{v} \cdot \nabla \bar{v} \right) = -\nabla p + \mu \nabla^2 \bar{v} + \bar{g} , \quad (1.2)$$

where,  $\bar{v}$  is the velocity vector,  $\rho$  is the fluid density,  $t$  is the time variable,  $p$  is the pressure,  $\mu$  is the dynamic viscosity of the fluid, and  $\bar{g}$  is the body force per unit volume. If the flow has a characteristic speed  $U$ , characteristic length  $L$ , and time  $T$ , then with all the variables in dimensionless form,  $\bar{v}^* = \bar{v}/U$ ,  $t^* = t/T$ ,  $p^* = p/(\rho U^2)$ ,  $\bar{g}^* = \bar{g}L/(\rho U^2)$ ,  $x^* = x/L$  and  $y^* = y/L$ , the governing equations become

$$\nabla^* \cdot \bar{v}^* = 0 , \quad (1.3)$$

$$\frac{k}{\pi} \frac{\partial \bar{v}^*}{\partial t^*} + \bar{v}^* \cdot \nabla^* \bar{v}^* = -\nabla^* p^* + \frac{1}{\text{Re}} \nabla^{*2} \bar{v}^* + \bar{g}^* , \quad (1.4)$$

where,  $k = \pi L/(UT)$  and  $\text{Re} = \rho UL/\mu$  which is the Reynolds number. For sinusoidal locomotion,  $U$  can be the moving speed,  $T$  the undulatory period which is  $1/f$  (frequency),  $L$  the chord length, then  $k$  is the reduced frequency  $k = \pi f L/U$ . For small Reynolds numbers, Eq. (1.4) is usually replaced with the Stokes equations, which have only viscous forces. For high Reynolds numbers, Eq. (1.4) will be replaced by potential flow which only considers inertial forces.

The propulsion of undulatory locomotion was first studied at low Reynolds numbers to understand how micro-organisms such as bacteria flagella propel their bodies in viscous fluids [5, 7, 25]. Though it was later found that bacteria flagellum spins helically rather than undulates in a 2-dimensional plane [23], there are two major theories applied to the understanding of the external forces by sinusoidal locomotion—the slender body theory and the resistive force theory.

The slender body theory was first introduced by Sir Geoffrey Taylor in 1951 [25] to solve the Stokes equation by singularity method. People are able to find the Green's function of the velocity field that meets the non-slip boundary condition on a slender

body [9, 13]. However, the Green's function solution is not very useful because it can only predict the velocity when the external forces acting on the body are known, and there is no analytical inverse solution that gives the external forces from the known velocity field. The velocity field can be experimentally measured, but the propulsive force is unknown. On the other hand, Gray and Hancock [5] introduced the resistive force theory to analyze the external forces on a slender body. The fundamental assumption of this theory is that the external forces are the resistive forces due to the movements. The magnitudes of resistive forces per unit length are given as  $f_n = C_n v_n$  in the normal direction and  $f_l = C_l v_l$  in the longitudinal direction.  $v_n$  and  $v_l$  are normal and longitudinal velocities, and  $C_n$  and  $C_l$  are normal and longitudinal resistive coefficients. The most important result of the resistive force theory is that, for a steady motion when the external force in the moving direction is zero, the ratio of moving speed to wave speed depends on  $C_n/C_l$  and the waveform  $2\pi A/\Lambda$  of the motion.  $C_n/C_l$  is a function of the geometry property of a slender body, and there are only estimated values of  $C_n/C_l$  for Newtonian fluids by the slender body theory [13]. Therefore, the propulsive force in general has not been revealed.

Although microscopic organisms operate at low Reynolds numbers (of the order of 1), other creatures performing sinusoidal undulation (such as snakes) can have larger Reynolds numbers. For example, a water snake of 1 m long which travels at a speed of its length per second will have the Reynolds number of  $10^6$  [22]. Thus, it is interesting to study sinusoidal motions at large enough Reynolds numbers to imply a condition of potential flow. The state-space airloads theory [17], which is based on potential flow with a non-penetration boundary condition, is applied to understanding the drag, lift and generalized forces on a thin flexible wing. The flexible wing is performing time-varying small deformations in a moving frame which can be experiencing large motions. The theory is formulated in terms of generalized deformations and generalized forces within that frame.

In the second part of the dissertation (Chapter 3), the state-space airloads theory is applied to calculate the propulsive force, lift and other generalized forces of sinusoidal locomotion at high Reynolds numbers. By giving a general kinetic equation of sinusoidal locomotion, explicit forms of all forces are found. In the discussion section, we will apply the experimental data to all these theories and compare.

### 1.3 The State-Space Airloads Theory

The state-space airloads theory [17] is a new but mature theory that was developed to calculate the forces for flexible, thin airfoils. This theory is based on potential flow with a non-penetration boundary condition in two dimensions. The thin airfoil can perform any small deformations with respect to a reference frame that can perform arbitrarily large translations and rotations. Thus, a moving coordinate system  $(x, y)$  is considered as illustrated in Fig. 1.2. The flow relative to the coordinate system at  $y = 0$ ,  $-b \leq x \leq b$  consists of a uniform  $x$ -velocity  $u_0$ , a uniform  $y$ -velocity  $v_0$ , and a gradient  $v_1$  due to the translations and rotations of the coordinate system. These velocity components can be time dependent. A thin airfoil of a chord length  $2b$  is performing small motions  $h(x, t)$  (positive down) with respect to the moving coordinates. Although the coordinate system itself can have arbitrarily large motion, the motions of the airfoil with respect to the coordinate system are assumed to be small, so that  $h \ll b$ ,  $\partial h/\partial x \ll 1$ ,  $\partial h/\partial t \ll u_0$ .

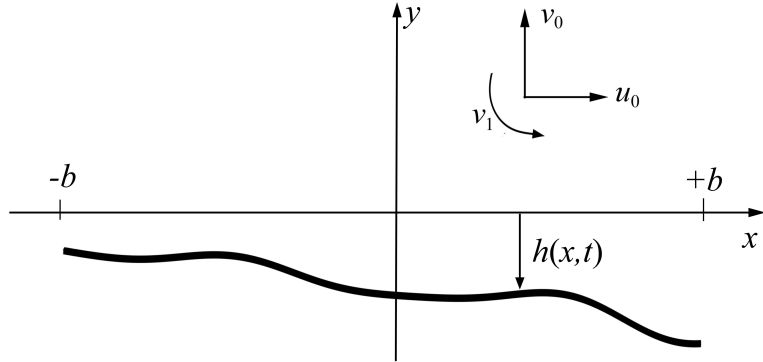


Figure 1.2: A general moving coordinate system for the state-space airloads theory.

In keeping with other thin airfoil theories, the non-penetration boundary condition is applied to the undeformed position of the airfoil on the  $x$ -axis with no loss of generality. The non-penetration boundary condition can be written as

$$w = \hat{v} + \lambda = u_0 \partial h / \partial x + \partial h / \partial t + v_0 + v_1 x / b, \quad (1.5)$$

where,  $w$  is the velocity of total induced flow,  $\lambda$  is the velocity of induced flow from the trailed circulation (positive down) and  $\hat{v}$  is the velocity of induced flow from bound circulation (positive down) necessary to enforce non-penetration of the surface.

The state-space airloads theory gives the generalized deformations and generalized forces in matrix forms. In order to use the results in matrix forms, all the variables need to be expanded in Glauert series. To do this, we have to introduce the Glauert change of variable,

$$x = b \cos \varphi, \quad -b \leq x \leq b, \quad 0 \leq \varphi \leq \pi, \quad (1.6)$$

where  $\varphi$  is the Glauert variable. Now, the motion of an airfoil can be written as the polynomial below,

$$h(x, t) = h(\varphi, t) = \sum_{n=0}^{\infty} h_n(t) \cos(n\varphi). \quad (1.7)$$

Note here, the expansion of  $\cos(n\varphi)$  are equivalent to the Chebyshev polynomials, and the coefficients of these terms can be found by following integrations,

$$h_0(t) = \frac{1}{\pi} \int_0^{\pi} h(\varphi, t) d\varphi, \quad (1.8)$$

$$h_n(t) = \frac{2}{\pi} \int_0^{\pi} h(\varphi, t) \cos(n\varphi) d\varphi, \quad (n \geq 1). \quad (1.9)$$

Similarly, we can expand other variables in Glauert series as Eq. (1.7). Now we can write the variables in matrix form. The elements of these matrices will be the coefficients of these Glauert series. That is,

$$\{h_n\} = \begin{pmatrix} h_0 \\ h_1 \\ h_2 \\ h_3 \\ \vdots \end{pmatrix}, \{L_n\} = \begin{pmatrix} L_0 \\ L_1 \\ L_2 \\ L_3 \\ \vdots \end{pmatrix}, \{v_n\} = \begin{pmatrix} v_0 \\ v_1 \\ 0 \\ 0 \\ \vdots \end{pmatrix}, \{\lambda_0\} = \begin{pmatrix} \lambda_0 \\ 0 \\ 0 \\ 0 \\ \vdots \end{pmatrix}, \{\lambda_1\} = \begin{pmatrix} \lambda_0 \\ \lambda_1 \\ 0 \\ 0 \\ \vdots \end{pmatrix}. \quad (1.10)$$

Eventually, the drag force per unit span  $D$ , generalized forces per unit span  $\{L_n\}$ , and total bound circulation per unit span  $\Gamma$  are given by the following equations.

$$\begin{aligned} \frac{1}{2\pi\rho}D = & -b\{\dot{h}_n + v_n - \lambda_0\}^T[\mathbf{S}]\{\dot{h}_n + v_n - \lambda_0\} \\ & + b\{\ddot{h}_n + \dot{v}_n\}^T[\mathbf{G}]\{h_n\} - u_0\{\dot{h}_n + v_n - \lambda_0\}^T[\mathbf{K} - \mathbf{H}]\{h_n\} \\ & + \{\dot{u}_0 h_n + \bar{u}_0 \zeta_n + u_0 v_n + u_0 \lambda_0\}^T[\mathbf{H}]\{h_n\}, \end{aligned} \quad (1.11)$$

$$\begin{aligned} \frac{1}{2\pi\rho}\{L_n\} = & -b^2[\mathbf{M}]\{\ddot{h}_n + \dot{v}_n\} - bu_0[\mathbf{C}]\{\dot{h}_n + v_n - \lambda_0\} \\ & - u_0^2[\mathbf{K}]\{h_n\} - b[\mathbf{G}]\{\dot{u}_0 h_n + \bar{u}_0 \zeta_n - u_0 v_n + u_0 \lambda_0\}, \end{aligned} \quad (1.12)$$

$$\frac{1}{\pi}\Gamma = b\{\mathbf{1}\}^T[\mathbf{C} - \mathbf{G}]\{\dot{h}_n + v_n - \lambda_1\} + u_0\{\mathbf{1}\}^T[\mathbf{K}]\{h_n\}, \quad (1.13)$$

where,

$$\{\mathbf{1}\} = \begin{pmatrix} 1 \\ 0 \\ 0 \\ 0 \\ 0 \\ \vdots \end{pmatrix}, \quad [\mathbf{K}] = \begin{pmatrix} 0 & 1 & 2 & 3 & 4 & \dots \\ 0 & -1/2 & 0 & 0 & 0 & \dots \\ 0 & 0 & -2/2 & 0 & 0 & \dots \\ 0 & 0 & 0 & -3/2 & 0 & \dots \\ 0 & 0 & 0 & 0 & -4/2 & \dots \\ \vdots & \vdots & \vdots & \vdots & \vdots & \ddots \end{pmatrix},$$

$$[\mathbf{C}] = \begin{pmatrix} 1 & 1 & 0 & 0 & 0 & \dots \\ -1/2 & 0 & 1/2 & 0 & 0 & \dots \\ 0 & -1/2 & 0 & 1/2 & 0 & \dots \\ 0 & 0 & -1/2 & 0 & 1/2 & \dots \\ 0 & 0 & 0 & -1/2 & 0 & \dots \\ \vdots & \vdots & \vdots & \vdots & \vdots & \ddots \end{pmatrix}, \quad [\mathbf{S}] = \begin{pmatrix} 1 & 0 & 0 & 0 & 0 & \dots \\ 0 & 0 & 0 & 0 & 0 & \dots \\ 0 & 0 & 0 & 0 & 0 & \dots \\ 0 & 0 & 0 & 0 & 0 & \dots \\ 0 & 0 & 0 & 0 & 0 & \dots \\ \vdots & \vdots & \vdots & \vdots & \vdots & \ddots \end{pmatrix},$$

$$[\mathbf{G}] = \begin{pmatrix} 0 & 1/2 & 0 & 0 & 0 & \dots \\ 0 & 0 & 1/4 & 0 & 0 & \dots \\ 0 & -1/4 & 0 & 1/4 & 0 & \dots \\ 0 & 0 & -1/4 & 0 & 1/4 & \dots \\ 0 & 0 & 0 & -1/4 & 0 & \dots \\ \vdots & \vdots & \vdots & \vdots & \vdots & \ddots \end{pmatrix}, [\mathbf{H}] = \begin{pmatrix} 0 & 0 & 0 & 0 & 0 & \dots \\ 0 & 1/2 & 0 & 0 & 0 & \dots \\ 0 & 0 & 2/2 & 0 & 0 & \dots \\ 0 & 0 & 0 & 3/2 & 0 & \dots \\ 0 & 0 & 0 & 0 & 4/2 & \dots \\ \vdots & \vdots & \vdots & \vdots & \vdots & \ddots \end{pmatrix},$$

and  $[\mathbf{M}]$  is tri-diagonal with

$$\mathbf{M}_{00} = 1/2, \mathbf{M}_{11} = 1/16, \mathbf{M}_{02} = \mathbf{M}_{20} = -1/4$$

$$\mathbf{M}_{nn} = \frac{n}{4(n^2 - 1)} \quad (n \geq 2),$$

$$\mathbf{M}_{n-1,n+1} = \mathbf{M}_{n+1,n-1} = 1/8n, \quad (n \geq 2).$$

Particularly,  $L_0$  is the lift force per unit span,  $L_1$  is the pitching moment per unit span, and  $L_2$  is the bending moment per unit span.



# Chapter 2

## Sinusoidal Locomotion of *C. elegans*

The locomotory behavior of *C. elegans* can be complicated. When crawling, *C. elegans* shows a relatively consistent sinusoidal wave. However, when it is swimming, its body displays “C” shapes and “S” shapes, which means its amplitude and wavelength could be changing during the undulation. In order to create an environment close to the ideal case of theoretical analysis, we focus on isolated *C. elegans* completely immersed in different fluids, including Newtonian solutions and non-Newtonian solutions. With the help of an original MATLAB image analysis program, we are able to see the underlying motion of *C. elegans* with digital analysis.

### 2.1 Experimental Setup and Procedure

There are many strains and mutants of *C. elegans*. We deal strictly with young adult hermaphrodites of the wild-type N2 strain. The young adult hermaphrodite *C. elegans* is around 1 mm long and can be obtained by culturing an “L4” stage larva at room temperature (22 °C) on a petri dish. An L4 stage larva can be recognized under a microscope because it has a brighter spot on its ventral side and is about half size of a mature adult [19]. A group of L4 *C. elegans* (15–20 worms) would be picked up and transferred to a fresh petri dish, where the worms were fed with *E. coli* OP50 bacteria to grow for 12–16 hours.

For each experiment, one young adult *C. elegans* is picked up by a worm picker put on a clean agar surface (no bacteria). The worm picker is made by mounting a 25 mm piece of 32 gauge (about 0.202 mm in diameter) platinum wire into the tip of a Pasture pipet. The worm is allowed to crawl on the surface for a few seconds to get rid of the bacteria on its body. After that, the worm is picked up by the picker again and put into a testing fluid. To reduce the impact from the worm picker and the environmental fluid, the worm is allowed to swim off the picker by slowly detaching itself from it. We waited about 2 minutes to start the video recording of its motion to ensure the worm is adapted to the environment and functions normal. A Lumenera microscope camera was used to record the motion of *C. elegans* at image size of 800 pixels by 800 pixels and a frame rate of 16 fps. For each testing fluid, at least three worms were recorded in three movie files. For each recorded movie, 6 to 12 clips of one complete period of undulation was analyzed.

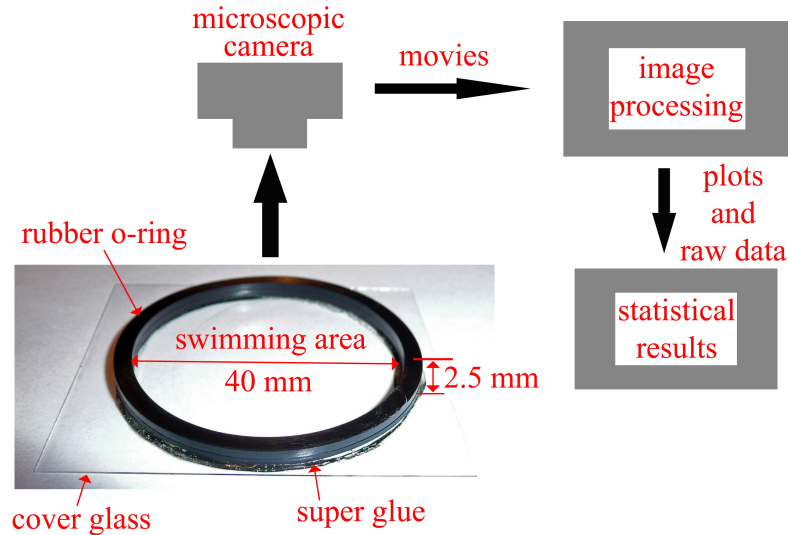


Figure 2.1: The experiment setup and procedure. A featureless device made of a rubber O-ring and a cover glass was used as the observation station of swimming *C. elegans*. A microscope camera was used to record the motion and the movies were analyzed by a MATLAB program.

Testing fluids were put in a device that is made of a rubber O-ring of 40 mm in diameter and 2.5 mm in depth on a smooth cover glass. Compared to the size of *C. elegans* (1 mm long and 0.08 mm wide), this device is considered large enough to neglect the boundary effects. Since the density of *C. elegans* is a little heavier

than that of water, it will sink to the bottom in water. However, for the testing fluids we used, *C. elegans* stayed in the vicinity of where it was dropped off. The testing fluids are Polyvinylpyrrolidone (PVP) aqueous solutions, and xanthan gum-PVP aqueous solutions. The PVP aqueous solutions were prepared by mixing certain weight percentage PVP (mol wt = 360,000, from Sigma-Aldrich) with D.I. water at room temperature (around 22°C) and stirring the mixture by a magnetic bar for 24 hours. Xanthan gum-PVP aqueous solutions were prepared by adding xanthan gum (from Sigma-Aldrich) to pre-mixed PVP aqueous solutions and stirring the mixture by a magnetic stirring bar for another 24 hours. Specifically, these testing fluids are 5 wt% PVP aqueous solution (5PVP), 8 wt% PVP aqueous solution (8PVP), 10 wt% PVP aqueous solution (10PVP), 1000 ppm xanthan gum (by weight) in 8 wt% PVP solution (8PVP-1000XG), 1000 ppm xanthan gum (by weight) in 10 wt% PVP solution (10PVP-1000XG), 2000 ppm xanthan gum (by weight) in 10 wt% PVP solution (10PVP-2000XG), 2500 ppm xanthan gum (by weight) in 10 wt% PVP solution (10PVP-2500XG), and 3000 ppm xanthan gum (by weight) in 10 wt% PVP solution (10PVP-3000XG). For simplification, we will use the short names of these solutions in the parentheses for the rest of this thesis. All testing solutions are set for 24–72 hours after mixed to release any pre-stress before the experiments.

The rheological properties of these solutions were tested using a TA Instruments AR 2000 stress controlled rheometer, primarily using a cone-and-plate geometry of 40 mm in diameter (cone angle 1°59'50", truncation 53  $\mu\text{m}$ ). A solution sample was put on the Peltier plate of the rheometer, the temperature of which was controlled at 22°C during the test. A solvent trap was used to minimize the evaporation of the sample. A series of steady shear test were performed to measure fluid viscosity, with shear rate from 0.01 s to 100 s. The steady flow procedure shows that PVP aqueous solutions having 10 wt% PVP or less have constant viscosity (Newtonian behavior), and xanthan gum-PVP solutions are shear-thinning. We also performed a series of small-amplitude oscillatory strain (SAOS) test to measure the viscoelastic properties of fluids. The results were plotted as storage modulus  $G'$  (solid-like behavior) and loss modulus  $G''$  (liquid-like behavior) versus angular frequency from 0.01 Hz to 1000 Hz. The angular frequency  $\omega^*$  where the first crossover of  $G'$  and  $G''$  occurs gives the longest relaxation time  $\tau_r$  of the solution, that is,  $\tau_r = 2\pi/\omega^*$  [15]. For pure viscous materials, the relaxation time is zero, but for pure elastic materials relaxation time can be viewed as infinity. Therefore, the longer  $\tau_r$ , the more elastic the material.

Table 2.1: Zero shear viscosity and relaxation time of the testing fluids.

testing fluids	zero viscosity $\mu_0$ [Pa.s]	relaxation time $\tau_r$ [sec]
5PVP	0.03	0.00
8PVP	0.12	0.79
10PVP	0.2	0.90
8PVP-1000XG	4.00	2.09
10PVP-1000XG	7.00	2.51
10PVP-2000XG	35.00	62.8
10PVP-2500XG	75.00	209.33
10PVP-3000XG	75.00	348.89

As shown in Table 2.1, zero shear viscosity indicates the viscosity of a fluid and relaxation time indicates the level of the elasticity of a fluid. The rheological analysis shows that 5PVP is Newtonian fluid, 8PVP and 10PVP are Bogor fluids (constant viscosity but elastic) [8], and all the xanthan gum-PVP fluids are shear thinning viscoelastic fluids. Generally, the concentration of PVP increases the fluid viscosity and the concentration of xanthan gum increases the fluid elasticity.

## 2.2 Data Analysis

The kinetic equation of a two dimensional undulatory locomotion of a slender body can be most simply approximated by a sine function in the  $y$  direction,

$$\begin{aligned}
 x(s, t) &= x(s, t_0) + g(s, t) , \\
 y(s, t) &= A \sin \left[ \frac{2\pi x(s, t_0)}{\Lambda} - 2\pi ft \right] . \tag{2.1}
 \end{aligned}$$

Here,  $s$  is the body coordinate along the centerline ( $0 \leq s \leq L$ ,  $s = 0$  is the head, and  $s = L$  is the tail),  $L$  the body length,  $t$  the time variable,  $t_0$  the initial time,  $A$  the amplitude,  $\Lambda$  the wavelength, and  $f$  the frequency.  $g(s, t)$  is not specified, which means the  $x$ -direction movement can be erratic. However, for steady progression in  $x$  direction it is usually assumed that the slender body has a constant moving speed for all parts of the body. That is,  $g(s, t) = V_m t$ , and  $V_m$  is defined as the moving speed

of the object. For general cases, the velocity of each body point is

$$v_x(s, t) = \frac{\partial x}{\partial t} = \frac{\partial g}{\partial t}, \quad (2.2)$$

$$v_y(s, t) = \frac{\partial y}{\partial t} = -2\pi Af \cos \left[ \frac{2\pi x(s, t_0)}{\Lambda} - 2\pi ft \right]. \quad (2.3)$$

From Eq. (2.2), we know  $x$ -velocity is not specified for sinusoidal locomotion but will contribute to the shape of the body. To investigate the details of the locomotion, we defined the time-averaged moving speed of each body point as  $V_m(s) = \int_{t_0}^{t_0+T} v_x(s, t) dt/T$ , and the moving speed of the whole object as  $V_m = \int_0^L V_m(s) ds/L$ . For the ideal case of steady progression in the  $x$  direction,  $v_x(s, t)$  will be constant and the body shape will be conserved in a same wave form. However, the body shape of swimming *C. elegans* is observed as “C” shapes and “S” shapes. To examine whether the locomotion of *C. elegans* is sinusoidal, we have to look at the  $y$ -velocity which should fit Eq. (2.3). Therefore, we developed an image and data analysis program, which is based on the edge-detection algorithm of MATLAB, to read the coordinates of the body centerline of *C. elegans*.

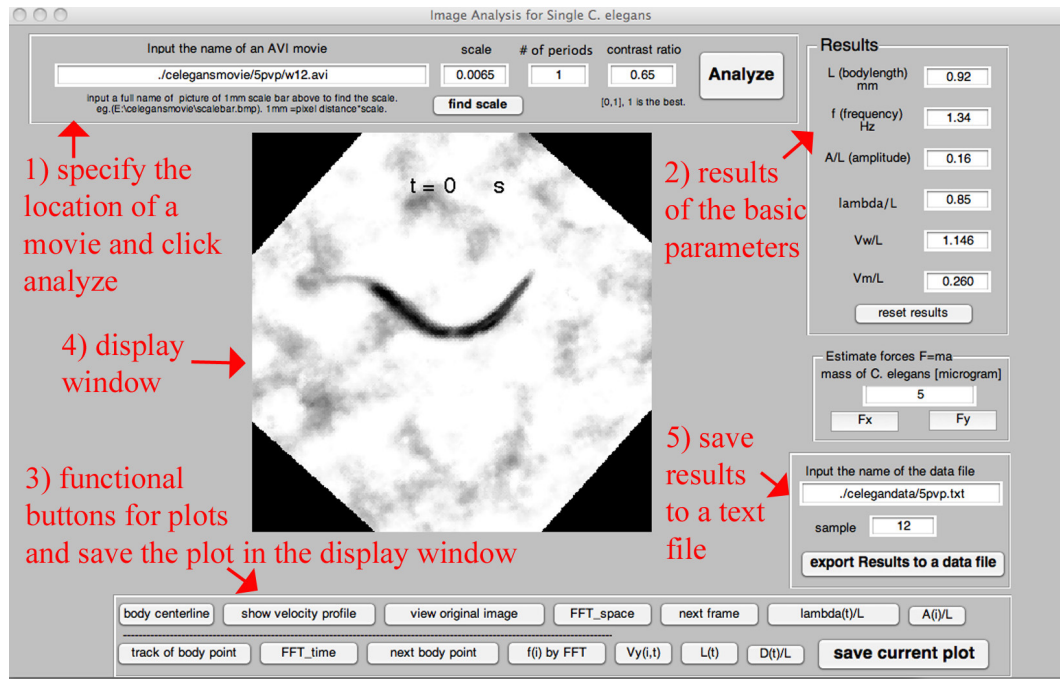


Figure 2.2: The user interface of the MATLAB image processing and data analysis program.

Our image analysis program can convert a movie clip containing integer periods  $n$  of undulation to the coordinates of 11 body points on the centerline. (The movie clip has to be in the “AVI” format). From head to tail, the coordinates of these body points are recorded as  $(x(i, m), y(i, m)), i = 1, 2, \dots, 11; m = 1, 2, \dots, N$ , where  $i$  is the body coordinate,  $m$  is the frame number, and  $N$  is the total number of frames. By knowing the coordinates of the body centerline of *C. elegans*, we can calculate the velocity of each body point as function of time.

$$v_x(i, m) = [x(i, m + 1) - x(i, m)]/\Delta t , \quad (2.4)$$

$$v_y(i, m) = [y(i, m + 1) - y(i, m)]/\Delta t , \quad (2.5)$$

where  $\Delta t$  is time interval between two consecutive frames.

With the image processing program, we are able to examine the details of the locomotory gaits, such as the body length at each frame  $L(m)$ , amplitude of each body point  $A(i)$ , and wavelength at each frame  $\Lambda(m)$ . The wavelengths are given by fast Fourier analysis of the body shape at each frame. The average amplitude of one undulatory period is given by  $A = \sum_{i=1}^{11} A(i)/11$ , and the average wavelength is given by  $\Lambda = \sum_{m=1}^N \Lambda(m)/N$ . The time-averaged moving speed of each body point over one undulation is defined as  $V_m(i) = [x(i, N) - x(i, 1)]/T$ , where  $T$  is the undulatory period, and the moving speed of the whole *C. elegans*  $V_m$  is defined as the average of  $V_m(i)$  that  $V_m = \sum_{i=1}^{11} V_m(i)/11$ .

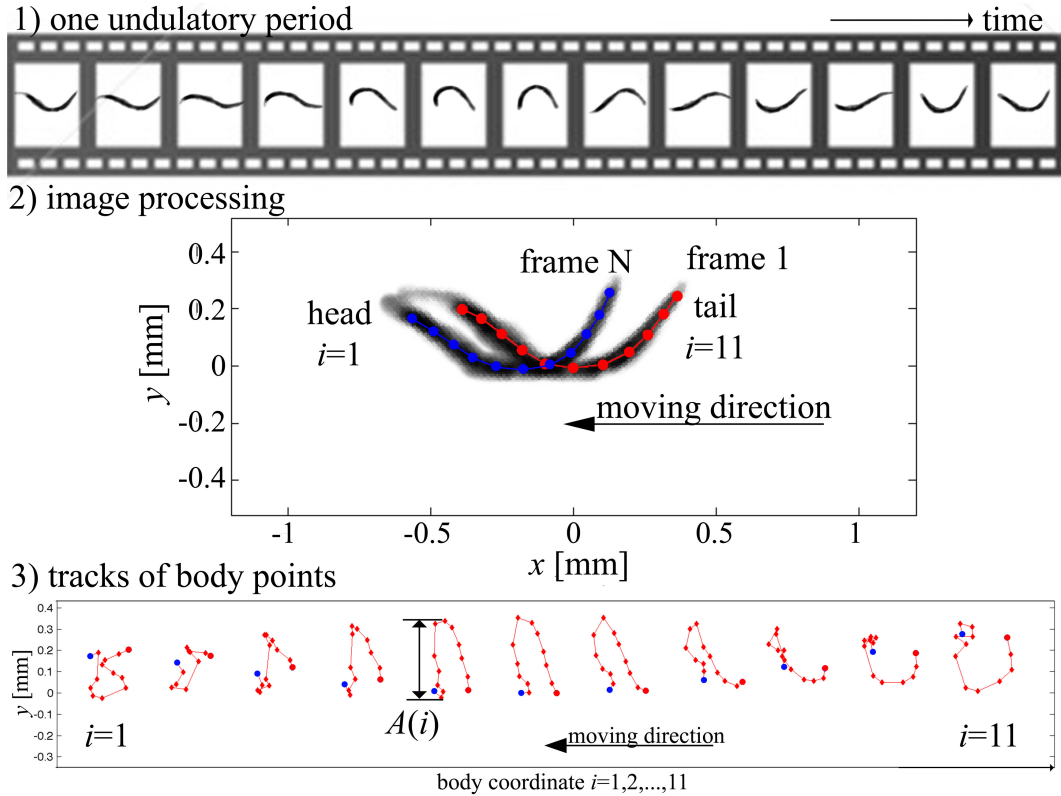


Figure 2.3: The procedure of image processing and data analysis. 1) A sequence of sinusoidal locomotion over one period is manually selected. Sample shown is from *C. elegans* in 5PVP. 2) After image processing, the coordinates of 11 body points (dots) are found for each frame. The first and last frame of the sequence are overlaid to find the moving direction and other important parameters. 3) Tracks of body points are used to find the amplitudes  $A(i)$ .

## 2.3 Results

### 2.3.1 The locomotory gaits of *C. elegans*

First, we learned that *C. elegans* keeps the same body length during crawling or swimming. Unlike an earthworm (*Lumbricus*), the body of which is very stretching, *C. elegans* has relatively stiff body in the longitudinal direction. This feature of *C. elegans* can be related to the alae, which are a pair of cuticular ridges along both sides

of its body.[3] For the purpose of comparison, our experimental results are normalized with the body length  $L$ . For example, we use normalized amplitude  $A/L$ , normalized wavelength  $\Lambda/L$ , and normalized moving speed  $V_m/L$ .

Second, we observed that the amplitude of each part of the body of swimming *C. elegans* is not consistent. As shown in Fig. 2.4, the middle part of the body has larger amplitude. However, crawling *C. elegans* keeps the same amplitude along its body. Third, the wavelength of a swimming *C. elegans* is also changing periodically with time, while for crawling *C. elegans* the wavelength is almost constant. Generally, the average amplitude and the average wavelength of swimming *C. elegans* are larger than those of crawling one. As the fluid becomes more viscoelastic, the deviations of both  $A(i)/L$  and  $\Lambda(t)/L$  become smaller.

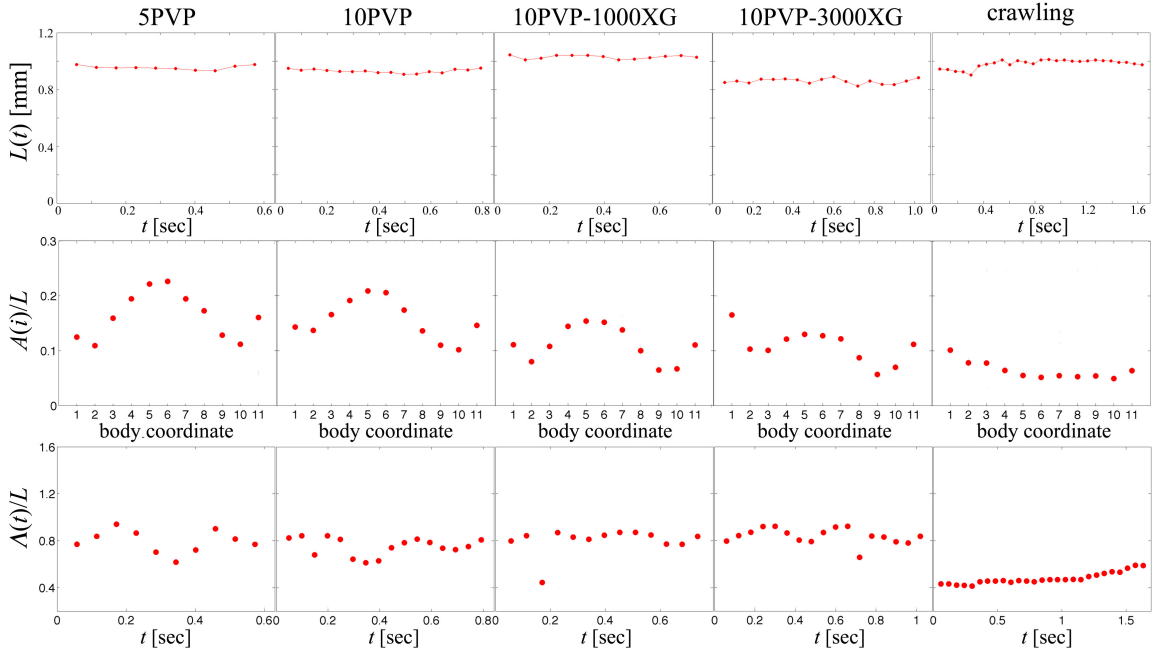


Figure 2.4: The body length, normalized amplitude, and normalized wavelength of *C. elegans* in 5PVP, 10PVP, 10PVP-1000XG, and 10PVP-3000XG. Only one sample is shown for each testing fluid. The data from crawling *C. elegans* (the last column on the right) are shown to compare with the swimming gaits.

We also examined the strokes at each frame,  $y$ -velocity of each body point  $v_y(i, m)/L$ , and time-averaged moving speed of each body points  $V_m(i)/L$ . We compared the experimental data with the standard equation of sinusoidal motion shown in Eq. (2.1). In Fig. 2.5, the computed results is for normalized amplitude of 0.17, normalized



wavelength of 0.88 and constant normalized moving speed of 0.25. These numbers are the averages of experimental data of *C. elegans* in 5 wt% PVP aqueous solution. Although the strokes of the swimming *C. elegans* are not as regular as the numerical prediction, one can still see the sinusoidal waveform *C. elegans* tries to follow.  $v_x$  is varying along the body and with time (results not shown), however, by filtering out the  $x$  direction noises, the contours of  $v_y$  also show that the locomotion has the form of wave propagation. Moreover, the time-averaged moving speed of each body point is almost constant along the body. For these reasons, we consider that the locomotion of *C. elegans* can be described by Eq. (2.1) with non-constant  $v_x(s, t)$ . The relatively erratic strokes of the body can be a result of slippage. However, when it is considered over one period time, we will use the average of  $V_m(i)$  to replace  $v_x$ .

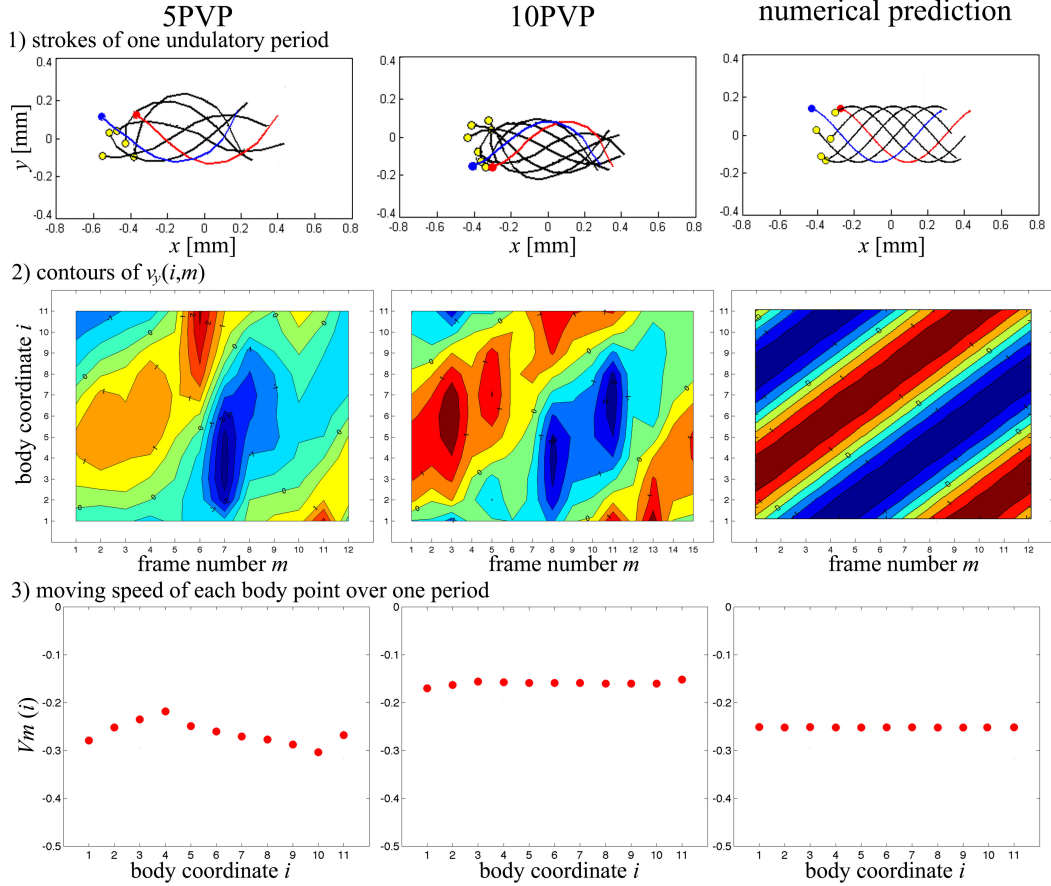


Figure 2.5: A comparison between the experimental data and computed data by Eqs. (2.1-2.3). The computed data is based on amplitude of 0.17, wavelength of 0.88, and moving speed 0.25 (the statistical results in 5PVP shown in Table 2.2). The contours of  $v_y(s,t)$  show the locomotory gaits of *C. elegans* is sinusoidal with consistent wavelength within the experimental errors.

### 2.3.2 Statistical results and viscoelastic effects

Karbowski et al., 2006 [10] studied the locomotion of crawling *C. elegans* (young adult wild-type N2 strain) and show that the average normalized wavelength is 0.62, the average normalized amplitude is 0.09, the average frequency is 0.36 Hz, and the average normalized moving speed 0.17. Korta et al., 2007 [11] studied the locomotory gaits of swimming *C. elegans* in Newtonian fluids. Their studies show that wavelength

of swimming *C. elegans* is around 0.9 of its body length for all viscous fluids they used, but the undulatory frequency drops 20% with every 10 fold increase of viscosity. In a very recent paper, Shen et al., 2011 [21] studied the undulation of *C. elegans* in viscoelastic fluids. They found the the moving speed of *C. elegans* in a viscoelastic fluid can decrease up to 35% of the moving speed when it is in a Newtonian fluid of the same viscosity.

Table 2.2: Statistical results of the locomotory data. # is the number of samples studied. The results are given as the average  $\pm$  the standard deviation.

testing fluids	#	$L$ [mm]	$f$ [Hz]	$A/L$	$\Lambda/L$	$V_m/L$
5PVP	19	$1.03 \pm 0.05$	$1.71 \pm 0.17$	$0.17 \pm 0.03$	$0.87 \pm 0.04$	$0.25 \pm 0.05$
8PVP	21	$0.85 \pm 0.07$	$1.50 \pm 0.20$	$0.14 \pm 0.01$	$0.88 \pm 0.05$	$0.17 \pm 0.04$
10PVP	27	$0.82 \pm 0.08$	$1.16 \pm 0.16$	$0.15 \pm 0.01$	$0.88 \pm 0.05$	$0.12 \pm 0.03$
8PVP-1000XG	23	$0.85 \pm 0.02$	$1.26 \pm 0.12$	$0.12 \pm 0.02$	$0.85 \pm 0.03$	$0.09 \pm 0.02$
10PVP-1000XG	25	$0.85 \pm 0.05$	$1.16 \pm 0.14$	$0.13 \pm 0.02$	$0.92 \pm 0.03$	$0.09 \pm 0.03$
10PVP-2000XG	17	$0.90 \pm 0.02$	$0.97 \pm 0.09$	$0.13 \pm 0.01$	$0.86 \pm 0.04$	$0.09 \pm 0.03$
10PVP-2500XG	13	$0.87 \pm 0.03$	$0.92 \pm 0.11$	$0.12 \pm 0.01$	$0.92 \pm 0.03$	$0.06 \pm 0.01$
10PVP-3000XG	22	$0.88 \pm 0.05$	$1.08 \pm 0.10$	$0.10 \pm 0.02$	$0.87 \pm 0.11$	$0.04 \pm 0.01$

Our testing fluids, except for 5PVP, are non-Newtonian. Particularly, 8PVP and 10PVP are Boger fluids, and others are shear thinning viscoelastic fluids. The basic parameters of sinusoidal locomotion are shown as the mean values and their standard deviations in Table 2.2. While we use zero shear viscosity  $\mu_0$  to characterize the viscosity of the fluid, we use Deborah numbers  $De$  to characterize the elasticity of the fluid. Deborah number is defined as the ratio of relaxation time and characteristic time of an experiment, so  $De = \tau_r f$  for sinusoidal locomotion. For non-elastic materials,  $De$  is zero.

Our results (in Fig. 2.6) show that the average wavelength of *C. elegans* is still a constant, around 0.9, in the range of  $\mu_0$  from 0.03 Pa·s to 75 Pa·s and the range of  $De$  from 0 to 300. The amplitude decreases slightly over the same wide ranges of  $\mu_0$  or  $De$ . It is not clear whether the viscosity or the elasticity affects the amplitude. But compare to the change in  $\mu_0$  or in  $De$ , we can almost neglect the change of amplitude.

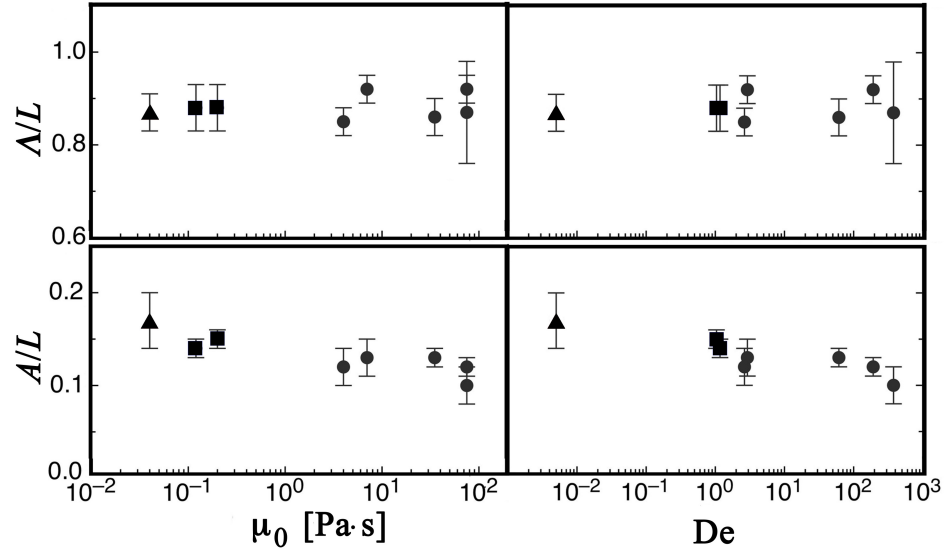


Figure 2.6: Normalized wavelength  $\Lambda/L$  and normalized wavelength  $A/L$  vs. zero shear viscosity  $\eta_0$  and Deborah number  $De$ . Triangles indicate Newtonian fluid (5PVP in this study), squares are Boger fluids (8PVP and 10PVP), and circles are viscoelastic fluids (all xanthan gum-PVP solutions). The error bars show the standard deviations.

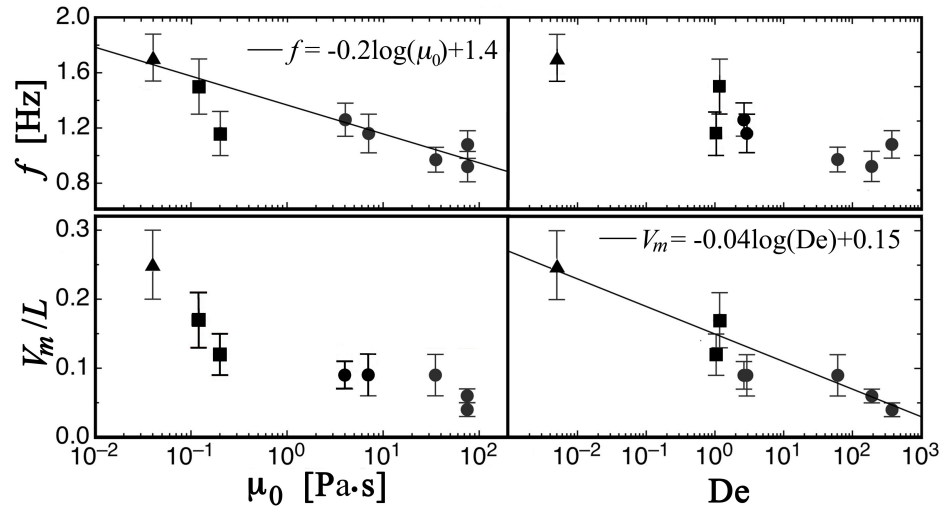


Figure 2.7: Frequency  $f$  and moving speed  $V_m/L$  vs. zero shear viscosity  $\eta_0$  and  $De$  number. Relations of  $f$ - $\eta_0$  and  $V_m$ - $De$  are shown to fit the experimental data. Triangles indicate the Newtonian fluids, squares are Boger fluids and circles are viscoelastic fluids.

As shown in Fig. 2.7, the experimental data of frequency distribute along the line  $f = -0.2 \log(\mu_0) + 1.4$  when plotted against  $\mu_0$ . This means the frequency  $f$  decreases 20% with every 10 fold increases of zero shear viscosity  $\mu_0$ , which is the same ratio as found in Korta's paper for Newtonian fluids. Therefore, the effect on undulatory frequency is due to the viscosity of fluids alone. However, the elasticity of fluids reduces the moving speed of *C. elegans*, and effect of fluid viscosity to the moving speed  $V_m$  are negligible. As the zero shear viscosity increases from 0.2 Pa·s to 35 Pa·s,  $V_m$  is almost constant. On the other hand, as seen in Fig. 2.7,  $V_m$  reduces 4% with every 10 fold increase in De number. That is,  $V_m = -0.04 \log(\text{De}) + 0.15$ .

### 2.3.3 Resistive coefficients of viscoelastic fluids

According to the resistive force theory, the ratio of the moving speed and the wave speed  $V_m/V_w$  is related to the ratio of resistive coefficients  $C_n/C_l$  and the wave form of a slender body. If we define  $K = C_n/C_l$ ,  $B = 2\pi A/\lambda$ , and  $\gamma = V_m/V_w$ , the equation of their relationship from the resistive force theory [5] is

$$\gamma = \frac{(K - 1)B^2}{2 + KB^2} . \quad (2.6)$$

From the slender body theory,  $K$  can be determined by the wavelength and radius of a slender body if it is for Newtonian fluids. In 1976, Sir James Lighthill gave an estimation of  $K$  for sinusoidal locomotion of a slender body in Newtonian fluids,

$$K = \frac{2 \log(2q/r)}{\log(2q/r) + 1/2} , \quad (2.7)$$

where  $q = 0.09\Lambda^*$  and  $\Lambda^*$  is the wavelength measured along the body [13] .

We can rewrite Eq. (2.6) as

$$1/\gamma = \frac{2}{K - 1} \frac{1}{B^2} + \frac{K}{K - 1} . \quad (2.8)$$

Since swimming *C. elegans* has almost constant wavelength, and if it is in Newtonian fluid, we should expect a linear relationship between  $1/\gamma$  and  $1/B^2$ . As shown in

Fig. 2.8, we do see the data distribute along a straight line for small De numbers ( $De < 20$ ). The best fit line by Eq. 2.8 shows  $K$  is around 1.4. We know the diameter of *C. elegans* is around 0.08 and  $\Lambda/L$  is around 0.9. Therefore, if  $r = 0.04$  and  $\Lambda^* = 1$ , Eq. (2.7) gives  $K \approx 1.13$ . However, Snztimann et al. [24] estimated the same  $K \approx 1.4$  from their experiments. In Gray and Lissmann's paper [6], they found  $C_n/C_l$  of golden syrup by measuring the settling velocity of small metal wires also around 1.4.

For large De numbers, the resistive force theory implies smaller  $K$ . We show the lines of the Eq. (2.8) with  $K = 1.28$  and  $K = 1.22$  in Fig. 2.8. There is not much known about the resistive coefficients of a slender body in viscoelastic fluids, neither experimentally nor theoretically. However, It is found that in viscoelastic fluids the resistive force of a spherical object is smaller than that in Newtonian fluids for the same settling velocity [12]. It is also found that the normal resistive force of a long cylinder is reduced in viscoelastic fluids [1]. Here, we propose a possible explanation. The elasticity of a viscoelastic fluid is due to polymers of long molecular chains, which can act like springs. These molecular springs can absorb part of the energy in the normal direction and result in less normal resistive force, but can not affect much in the longitudinal direction. That is,  $C_n$  become smaller when fluid is elastic, so is  $K = C_n/C_l$ .

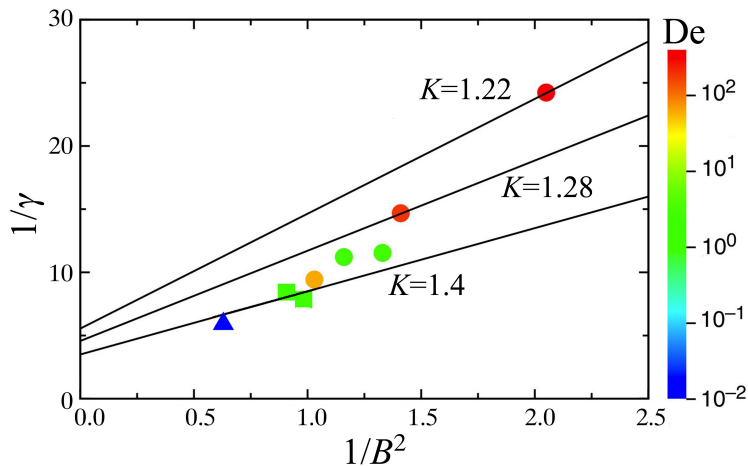


Figure 2.8:  $1/\gamma$  vs.  $1/B^2$ . The markers (triangle, squares and circles) are the means of the experimental data for each testing fluid. The values of De number is indicated by the color. The solid lines are the theoretical prediction by the resistive force theory with different  $K$  values. The slope of the lines is given by  $2/(K - 1)$  and the constant is  $K/(K - 1)$ .

# Chapter 3

## Propulsion by Sinusoidal Locomotion at High Reynolds Numbers

### 3.1 Coordinate System and Equation of Sinusoidal Motions

A coordinate system  $x$ - $y$  is considered moving in the negative  $x$ -axis direction at a speed of  $u_0$  in a mass of still fluid or air. A thin flexible wing of chord length  $2b$  and span length  $S$  is making a sinusoidal wave in this moving coordinate system. The wing is moving up and down on the  $y$ -axis with a maximum amplitude  $A$ . The sinusoidal wave is propagating in the  $x$ -axis direction with a wavelength  $\Lambda$  and a frequency  $f$ . In this paper, we neglect the small changes along the span direction and focus on the motion on the  $x$ - $y$  plane as shown in Fig. 3.1. Since the  $x$ - $y$  plane is moving to its left at a speed of  $u_0$ , the flow relative to the  $x$ - $y$  coordinate system at  $y = 0$ ,  $-b \leq x \leq b$  only consists of a uniform  $x$ -velocity  $u_0$ . We assume  $A/(2b) \ll 1$  and the projection of the wing on the  $x$ -axis is fixed as  $2b$  for the purpose of applying the non-penetration boundary condition. Thus, the deformation of a flexible wing performing sinusoidal motion in two dimensions is

$$h(x, t) = -A \sin\left(\frac{2\pi x}{\Lambda} - 2\pi f t\right), \quad (3.1)$$

where  $A$  is the amplitude,  $\Lambda$  is the wavelength,  $f$  is the frequency, and  $t$  is time.

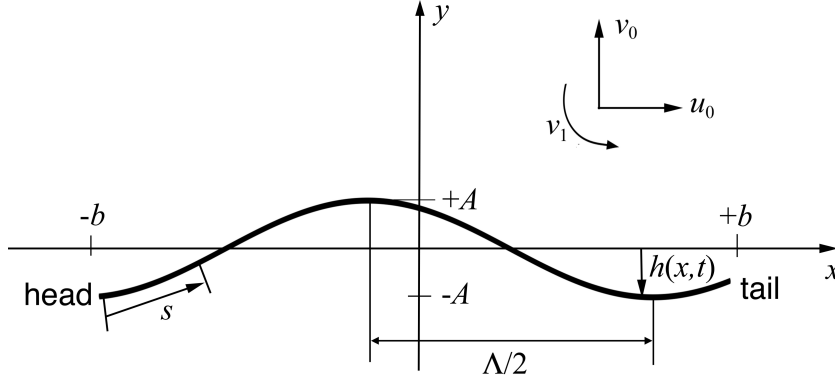


Figure 3.1: A 2D coordinate system of a flexible wing performing sinusoidal locomotion.  $v_0$  and  $v_1$  are zeros here.

After a Glauert change of variables shown in Eq. (1.6), the equation of motion can be expressed as the polynomial below,

$$h(\varphi, t) = -A \sin\left(\frac{\pi \cos \varphi}{z} - \omega t\right) = \sum_{n=0}^{\infty} h_n(t) \cos(n\varphi), \quad (3.2)$$

where,  $z = \Lambda/(2b)$  is the dimensionless wavelength, and  $\omega = 2\pi f$  is the angular frequency. The expansion terms of  $\cos(n\varphi)$  are equivalent to the Chebyshev polynomials, and the coefficients of these terms can be found by doing the integrations in Eqs. (1.8-1.9). Applying Eq. (3.2) to the integrals in Eq. (1.8-1.9), that

$$\begin{aligned} h_0(t) &= -\frac{1}{\pi} \int_0^{\pi} A \sin\left(\frac{\pi}{z} \cos \varphi - \omega t\right) d\varphi \\ &= \frac{A}{\pi} \left[ -\cos(\omega t) \int_0^{\pi} \sin\left(\frac{\pi}{z} \cos \varphi\right) d\varphi + \sin(\omega t) \int_0^{\pi} \cos\left(\frac{\pi}{z} \cos \varphi\right) d\varphi \right], \end{aligned} \quad (3.3)$$

$$\begin{aligned} h_n(t) &= -\frac{2}{\pi} \int_0^{\pi} A \sin\left(\frac{\pi}{z} \cos \varphi - \omega t\right) \cos(n\varphi) d\varphi \quad (n \geq 1) \\ &= \frac{2A}{\pi} \left[ -\cos(\omega t) \int_0^{\pi} \sin\left(\frac{\pi}{z} \cos \varphi\right) \cos(n\varphi) d\varphi + \sin(\omega t) \int_0^{\pi} \cos\left(\frac{\pi}{z} \cos \varphi\right) \cos(n\varphi) d\varphi \right]. \end{aligned} \quad (3.4)$$



Note that, the integrals in Eqs. (3.3-3.4) are Bessel integrals [4], whose values are

$$\int_0^\pi \sin\left(\frac{\pi}{z} \cos \varphi\right) \cos(n\varphi) \, d\varphi = \pi \sin\left(\frac{n\pi}{2}\right) J_n\left(\frac{\pi}{z}\right), \quad (3.5)$$

$$\int_0^\pi \cos\left(\frac{\pi}{z} \cos \varphi\right) \cos(n\varphi) \, d\varphi = \pi \cos\left(\frac{n\pi}{2}\right) J_n\left(\frac{\pi}{z}\right), \quad (3.6)$$

where  $J_n$  are Bessel functions of the first kind ( $n$  are integers). Therefore,  $h_n(t)$  ( $n \geq 0$ ) are simplified to

$$h_0(t) = AJ_0\left(\frac{\pi}{z}\right) \sin(\omega t), \quad (3.7)$$

$$h_n(t) = 2AJ_n\left(\frac{\pi}{z}\right) \left[ -\sin\left(\frac{n\pi}{2}\right) \cos(\omega t) + \cos\left(\frac{n\pi}{2}\right) \sin(\omega t) \right], \quad (n \geq 1). \quad (3.8)$$

Let us write these  $\{h_n\}$  in an uniform format of  $\cos(\omega t)$  and  $\sin(\omega t)$ ,

$$\{h_n\} = b\{\alpha_n\} \cos(\omega t) + b\{\beta_n\} \sin(\omega t), \quad (n \geq 0). \quad (3.9)$$

If we compare Eq. (3.9) to Eq. (3.7-3.8), then

$$\begin{aligned} \alpha_0 &= 0, & \beta_0 &= \frac{A}{b} J_0\left(\frac{\pi}{z}\right), \\ \alpha_n &= -\frac{2A}{b} \sin\left(\frac{n\pi}{2}\right) J_n\left(\frac{\pi}{z}\right), & \beta_n &= \frac{2A}{b} \cos\left(\frac{n\pi}{2}\right) J_n\left(\frac{\pi}{z}\right), \quad (n \geq 1). \end{aligned} \quad (3.10)$$

In this way, the time-derivatives of  $\{h_n\}$  can also be written in the same format.

$$\{\dot{h}_n\} = b\omega\{\beta_n\} \cos(\omega t) - b\omega\{\alpha_n\} \sin(\omega t), \quad (n \geq 0), \quad (3.11)$$

$$\{\ddot{h}_n\} = -b\omega^2\{\alpha_n\} \cos(\omega t) - b\omega^2\{\beta_n\} \sin(\omega t), \quad (n \geq 0). \quad (3.12)$$

## 3.2 Propulsion, Lift and Generalized Forces

A positive propulsive force for the sinusoidal locomotion will be the drag force in the negative  $x$ -axis direction. Therefore, a dimensionless propulsive coefficient is defined as

$$C_F = -\frac{D}{2\pi\rho b u_0^2}, \quad (3.13)$$

where,  $D$  is the drag force per unit span in Eq. (1.11), and  $\rho$  is the density of environmental fluid or air. At certain reduced frequencies  $k = \omega b/u_0$ , there will be shed vortices. In order to separate the effect of shed vorticity, we will use the following notation

$$C_{F-\text{with wake}} = C_{F-\text{no wake}} - \Delta C_F, \quad (3.14)$$

where  $C_{F-\text{with wake}}$  is the coefficient of propulsion with the existence of shed vortices,  $C_{F-\text{no wake}}$  is the coefficient of propulsion without shed vorticity effects, and  $\Delta C_F$  is the loss of propulsion due to shed vorticity alone.

By applying Eq. (1.11) to Eq. (3.13) and separating the effect of shed vorticity, we will have

$$C_{F-\text{no wake}} = \frac{\dot{h}_0^2}{u_0^2} - \frac{1}{4u_0^2} \left[ \ddot{h}_0 h_1 + \sum_{n=1}^{\infty} (\ddot{h}_{n-1} - \ddot{h}_{n+1}) h_n \right] + \frac{1}{u_0} \sum_{n=1}^{\infty} n(\dot{h}_0 - \dot{h}_n) h_n / b, \quad (3.15)$$

$$\Delta C_F = 2 \frac{\lambda_0 \dot{h}_0}{u_0^2} + \frac{\lambda_0}{u_0} \sum_{n=1}^{\infty} n h_n / b - \frac{\lambda_0^2}{u_0^2}, \quad (3.16)$$

where  $\lambda_0$  is the velocity due to shed vorticity.

Similarly, we also define a coefficient of lift as  $C_L = L_0/(2\pi\rho b u_0^2)$ , a coefficient of pitching moment as  $C_{L1} = L_1/(2\pi\rho b u_0^2)$ , and a coefficient of bending moment as  $C_{L2} = L_2/(2\pi\rho b u_0^2)$ .  $L_0$  is the lift force per unit span,  $L_1$  is the pitching moment per unit span, and  $L_2$  is the bending moment per unit span. We use the same notation as for propulsive coefficient and apply Eq. (1.12), the coefficients of lift and generalized forces are

$$C_{L-\text{no wake}} = -\frac{b}{4u_0^2} (2\ddot{h}_0 - \ddot{h}_2) - \frac{1}{u_0} (\dot{h}_0 + \dot{h}_1) - \sum_{n=1}^{\infty} n h_n / b, \quad (3.17)$$

$$\Delta C_L = -\frac{\lambda_0}{u_0}, \quad (3.18)$$

$$C_{L1-\text{no wake}} = -\frac{b}{16u_0^2} (\ddot{h}_1 - \ddot{h}_3) + \frac{1}{2u_0} (\dot{h}_0 - \dot{h}_2) - \frac{1}{2} h_1 / b, \quad (3.19)$$

$$\Delta C_{L1} = \frac{\lambda_0}{2u_0}, \quad (3.20)$$

$$C_{L2-\text{no wake}} = -\frac{b}{24u_0^2}(-6\ddot{h}_0 + 4\ddot{h}_2 - \ddot{h}_4) + \frac{1}{2u_0}(\dot{h}_1 - \dot{h}_2) - \frac{1}{2}h_1/b , \quad (3.21)$$

$$\Delta C_{L2} = 0 . \quad (3.22)$$

When applying  $\{h_n\}$ ,  $\{\dot{h}_n\}$  and  $\{\ddot{h}_n\}$  of sinusoidal locomotion, Eqs. (3.9-3.12) to Eqs. (3.15-3.22), there will be summations of  $n\alpha_n$ ,  $n\beta_n$ ,  $n(\alpha_n^2 - \beta_n^2)$  and  $n\alpha_n\beta_n$  from  $n = 1$  to infinity. These summations can be greatly simplified for the case of sinusoidal locomotion, because of the special property of Bessel functions of the first kind that  $J_n(x) = x[J_{n-1}(x) + J_{n+1}(x)]/(2n)$  [4]. In particular,

$$\begin{aligned} \sum_{n=1}^{\infty} n\alpha_n &= -k_0\beta_0 , \\ \sum_{n=1}^{\infty} n\beta_n &= \frac{1}{2}k_0\alpha_1 , \\ \sum_{n=1}^{\infty} n(\alpha_n^2 - \beta_n^2) &= -k_0\alpha_1\beta_0 , \\ \sum_{n=1}^{\infty} n\alpha_n\beta_n &= 0 , \end{aligned} \quad (3.23)$$

where  $k_0 = \pi/z$ . The derivations of these identities are shown in appendix A.

### 3.2.1 Case of no shed vorticity

First we consider a special case when there is no shed vorticity effects, that is,  $\lambda_0$  is zero. For simplification, we will use reduced frequency  $k = \omega b/u_0$ , reduced time  $\tau = u_0 t/b$ , and critical reduced frequency  $k_0 = \pi/z$ . With these definitions,  $\omega t = k\tau$  in the harmonic functions. We are able to obtain very simple closed forms of the coefficients of all forces for sinusoidal motions. They are

$$C_{F-\text{no wake}} = (k - k_0)k\beta_0 \left[ \beta_0 \cos^2(k\tau) + \frac{\alpha_1}{2} \cos(k\tau) \sin(k\tau) \right] , \quad (3.24)$$

$$C_{L-\text{no wake}} = -(k - k_0) \left[ \beta_0 \cos(k\tau) + \frac{\alpha_1}{2k_0} (k - k_0) \sin(k\tau) \right] , \quad (3.25)$$

$$C_{L1-\text{no wake}} = \frac{(k - k_0)}{2k_0} \left[ \left( \frac{\alpha_1}{k_0} - \beta_0 \right) k - \alpha_1 \right] \cos(k\tau) , \quad (3.26)$$

$$C_{L2-\text{no wake}} = 2 \frac{(k - k_0)^2}{k_0^2} \left( \frac{\alpha_1}{k_0} + \beta_0 \right) \sin(k\tau) . \quad (3.27)$$

These forces are time-dependent and oscillate as sinusoidal functions of time. When  $k = k_0$ , all forces are zero. Therefore, we call  $k_0$  the critical reduced frequency. Note here,  $\alpha_1 = -2(A/b)J_1(k_0)$  and  $\beta_0 = (A/b)J_0(k_0)$ , so the coefficients without shed vorticity effects depend on amplitude  $A$ , critical reduced frequency  $k_0$ , and reduced frequency  $k$ .  $C_{F-\text{no wake}}$  is a function of  $(A/b)^2$  and other coefficients are in linear relationships with  $A/b$ . However, since we have assumed a moderate amplitude to be able to apply a non-penetration boundary condition, we will not consider the amplitude  $A/b$  greater than 0.2.

### 3.2.2 Shed vorticity effects

As the Reynolds number increases, a laminar flow will transit into a turbulent flow. Since sinusoidal motion is time-dependent, this transition is also related to the reduced frequency  $k = \omega b/u_0$ , which represents the ratio of the motion in the transverse direction and the motion in the moving direction. In the actual motion at reduced frequency  $k$ , there will be shed vortices. We use Theodorsen theory [26] to find  $\lambda_0$ , the velocity due to shed vorticity.

$$\begin{aligned} \lambda_0 &= \text{Re}[\bar{\lambda}_0 e^{ik\tau}] , \\ \bar{\lambda}_0 &= (\bar{w}_0 + \frac{1}{2}\bar{w}_1)[1 - C(k)] , \end{aligned} \quad (3.28)$$

where  $\bar{\lambda}_0$ ,  $\bar{w}_0$ ,  $\bar{w}_1$ , and  $C(k)$  are complex numbers [16]. The term  $\bar{w}_0 + \bar{w}_1/2$  is the complex form of total velocity components,  $w_0 + w_1/2$ , which can also be expressed in the components of motion [17], that is

$$\begin{aligned} w_0 + \frac{1}{2}w_1 &= \text{Re}[(\bar{w}_0 + \frac{1}{2}\bar{w}_1)e^{ik\tau}] \\ &= \dot{h}_0 + \frac{1}{2}\dot{h}_1 + u_0 \sum_{n=1}^{\infty} nh_n/b . \end{aligned} \quad (3.29)$$

$C(k)$  is the Theodorsen function. Let  $1 - C(k) = M(k) + N(k)i$ , where the numerical values of  $M(k)$  and  $N(k)$  can be approximated as

$$M(X) = 0.5 - 0.5(1 - X)^4 - 0.1X(1 - X)^2 - 0.152X(1 - X)^3 + 0.47X(1 - X)^4, \quad (3.30)$$

$$N(X) = -X \ln(X)(1 - X)^3 + 0.0905X(1 - X) + 0.609X(1 - X)^2 - 0.686X(1 - X)^3, \quad (3.31)$$

where  $X = k/(k + 1)$  [18]. Figure 3.2 shows the value of  $M$  and  $N$  as functions of  $X$ . At  $X = 0$ ,  $k = 0$ , and  $X = 1$ ,  $k = \infty$ .

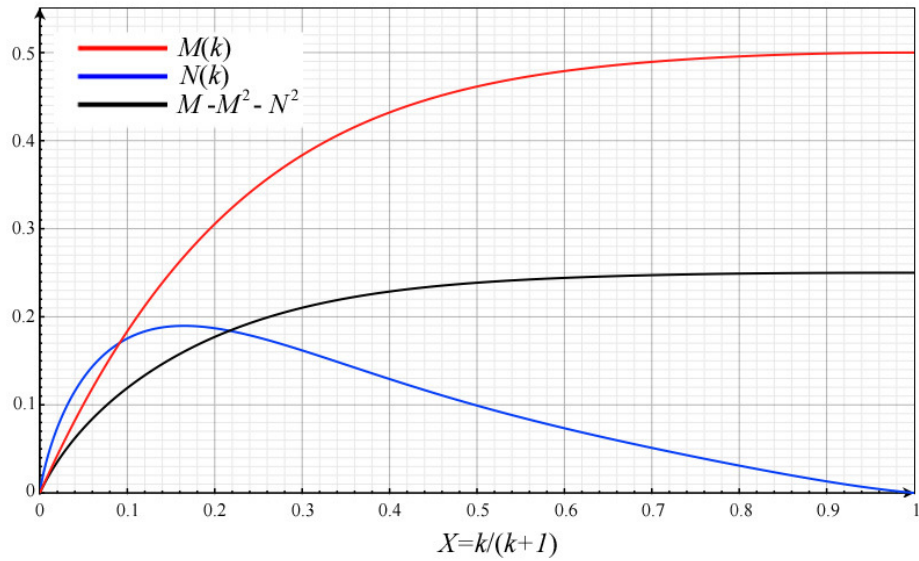


Figure 3.2: Numerical approximation of  $M(k)$  and  $N(k)$  verse scaled reduced frequency  $k/(k + 1)$ . The value of  $M - M^2 - N^2$ , which is a factor in lost power  $\overline{C_W}$ , is also shown.

Combine Eqs. (3.28-3.31) and components of motion in Eq. (3.9), the velocity due to shed vorticity for a sinusoidal motion at reduced frequency  $k$  is found to be

$$\frac{\lambda_0}{u_0} = (k - k_0) \left[ (M\beta_0 - \frac{1}{2}N\alpha_1) \cos(k\tau) + (-\frac{1}{2}M\alpha_1 - N\beta_0) \sin(k\tau) \right]. \quad (3.32)$$

For simplification, we rewrite Eq. (3.32) as

$$\frac{\lambda_0}{u_0} = (k - k_0) [\lambda_\alpha \cos(k\tau) + \lambda_\beta \sin(k\tau)]. \quad (3.33)$$

where  $\lambda_\alpha = M\beta_0 - N\alpha_1/2$  and  $\lambda_\beta = -M\alpha_1/2 - N\beta_0$ . As shown in Eq. (3.33), the ratio of velocity due to shed vorticity and moving speed of the wing has zero mean over one undulation, but its amplitude is increasing with the reduced frequency  $k$ . At  $k = k_0$ , there is no shed vorticity.

Replacing the value of  $\lambda_0/u_0$  in Eq. (3.16), Eq. (3.18) and Eq. (3.20) with Eq. (3.33), we are able to derive the closed forms of the force losses due to shed vorticity,

$$\begin{aligned} \Delta C_F = & (k - k_0) \left\{ [(2\lambda_\alpha\beta_0 - \lambda_\alpha^2)k - (\lambda_\alpha^2 - \lambda_\alpha\beta_0)k_0] \cos^2(k\tau) \right. \\ & + [(2\lambda_\beta\beta_0 - 2\lambda_\alpha\lambda_\beta)k - (\lambda_\beta\beta_0 - \frac{1}{2}\lambda_\alpha\alpha_1 + 2\lambda_\alpha\lambda_\beta)k_0] \cos(k\tau) \sin(k\tau) \\ & \left. + [-\lambda_\beta^2k + (\frac{1}{2}\lambda_\beta\alpha_1 + \lambda_\beta^2)k_0] \sin^2(k\tau) \right\}, \end{aligned} \quad (3.34)$$

$$\Delta C_L = -(k - k_0)[\lambda_\alpha \cos(k\tau) + \lambda_\beta \sin(k\tau)], \quad (3.35)$$

$$\Delta C_{L1} = \frac{1}{2}(k - k_0)[\lambda_\alpha \cos(k\tau) + \lambda_\beta \sin(k\tau)]. \quad (3.36)$$

At  $k = k_0$ , Eqs. (3.34-3.36) become zero. This is in agreement with the fact that when  $C_L = 0$  (at  $k = k_0$ ) there is no shed vorticity.

### 3.2.3 Time-averaged propulsion

Since all the forces are time dependent and periodical, it is important to know their time-averaged values over one undulatory period. In Eq. (3.24-3.27) and Eq. (3.34-3.36), the propulsive force has only terms of  $\cos^2(k\tau)$ ,  $\sin^2(k\tau)$  and  $\cos(k\tau) \sin(k\tau)$ . The other forces are functions of  $\cos(k\tau)$  and  $\sin(k\tau)$ . Since the time average of  $\cos(k\tau)$  and  $\sin(k\tau)$  are zero, so the time-averaged lift and generalized forces are zero. However,  $\cos^2(k\tau)$  is  $[1 + \cos(2k\tau)]/2$  and its time average is  $1/2$ . Similarly, the time average of  $\sin^2(k\tau)$  is  $1/2$ , and  $\cos(k\tau) \sin(k\tau)$  is 0. Let us note the time-averaged propulsion as  $\overline{C_{F-\text{no wake}}}$  and  $\Delta\overline{C_F}$ , and they are

$$\overline{C_{F-\text{no wake}}} = \frac{1}{2}k(k - k_0)\beta_0^2, \quad (3.37)$$

$$\begin{aligned} \Delta \overline{C}_F &= \frac{k - k_0}{2} \left\{ [2M\beta_0^2 - N\alpha_1\beta_0 - (M^2 + N^2)(\beta_0^2 + \frac{\alpha_1^2}{4})]k \right. \\ &\quad \left. + (M^2 + N^2 - M)(\beta_0^2 + \frac{\alpha_1^2}{4})k_0 \right\} . \end{aligned} \quad (3.38)$$

For the case of no shed vorticity, the propulsive force is determined by  $k$  and  $\beta_0$ . When  $\beta_0$  is not zero, there will be positive time-averaged propulsive force for  $k$  greater than  $k_0$ . When  $z = 0.569$  and  $z = 1.3$ , the Bessel function  $J_0(\pi/z)$  in  $\beta_0$  is zero, so  $\overline{C}_{F-\text{no wake}}$  is zero regardless of the value of  $k$ . At  $z = 0.82$ , where  $J_0(\pi/z)$  is at its extreme, the system achieves the maximum propulsion for a fixed  $k$ . The shed vorticity will affect the time-averaged propulsion by the input of  $\alpha_1$ , which has  $J_1(\pi/z)$ . As  $k$  approaches infinity,  $M = 0.5$  and  $N = 0$  (shown in Fig. 3.2), the effect due to shed vorticity on propulsion is very close to

$$\Delta \overline{C}_F = \frac{1}{2} \left( \frac{3}{4} \beta_0^2 - \frac{\alpha_1^2}{16} \right) k^2 . \quad (3.39)$$

by comparing Eq. 3.39 to Eq. 3.37, we found that at large  $k$ , the total propulsive force can be approximated as

$$\overline{C}_{F-\text{with wake}} = \frac{1}{8} \left( \beta_0^2 + \frac{\alpha_1^2}{4} \right) k^2 . \quad (3.40)$$

### 3.3 Propulsive Efficiency

We are now in a position to investigate the propulsive efficiency of warping airfoils at high Reynolds numbers. We begin with calculation of the power required for the airfoil to make its deformations. This can be found by the dot product of generalized velocities with generalized forces,

$$P = -\{\dot{h}_n\}^T \{L_n\} , \quad (3.41)$$

where positive  $P$  implies work done on the airflow and negative  $P$  would imply energy taken out of the free-stream (an energy-extraction device). Therefore, the applied

power coefficient,  $C_P = P/(2\pi\rho b u_0^3)$ , is given by:

$$C_P = \{h'_n\}^T [\mathbf{M}] \{h''_n\} + \{h'_n\}^T [\mathbf{C}] \{h'_n - \lambda_0\} + \{h'_n\}^T [\mathbf{K}] \{h_n\} , \quad (3.42)$$

where (for simplicity)  $u_0 = b = 1$  and the symbol  $( )'$  implies a derivative with respect to reduced time  $\tau$ . Matrices  $[\mathbf{M}]$ ,  $[\mathbf{C}]$ , and  $[\mathbf{K}]$  are defined in the state-space airloads theory and given in Chapter 1.3.

Since the motion is simple and harmonic, we are only interested in the time-averaged power over one undulation. Therefore, there are several terms that have zero time average can be eliminated from Eq. (3.42). Also, there are some terms in that equation which can be expressed as a time-derivative of a single quantity. For example, due to the symmetry of matrix  $[\mathbf{M}]$

$$\{h'_n\}^T [\mathbf{M}] \{h''_n\} = \frac{1}{2} [\{h'_n\}^T [\mathbf{M}] \{h'_n\}]' . \quad (3.43)$$

With this simplification and the definitions of the matrices, the time-averaged power required for the wing motion,  $\overline{C_P}$ , is

$$\overline{C_P} = (h'_0)^2 + \frac{1}{2} h'_0 h'_1 + \frac{1}{2} h'_0 \sum_{n=1}^{\infty} n h_n - \frac{1}{2} h_0 \sum_{n=1}^{\infty} n h'_n - h'_0 \lambda_0 + \frac{1}{2} h'_1 \lambda_0 . \quad (3.44)$$

After application of the expansions for the  $\{h_n\}$  and taking the time average, the final form of the input power coefficient is given by:

$$\overline{C_P} = \frac{1}{2} k(k - k_0) \beta_0^2 - \frac{1}{2} k(k - k_0) [M \beta_0^2 - M \frac{\alpha_1^2}{4} - N \alpha_1 \beta_0] . \quad (3.45)$$

Because the useful propulsive power is  $u_0 F$ , the propulsive power coefficient is identical to the propulsive force coefficient  $C_F$ . Thus, we define the time average of propulsive power coefficient as  $\overline{C_F}$ , and

$$\begin{aligned} \overline{C_F} = & \frac{1}{2} k(k - k_0) \beta_0^2 - \frac{1}{2} (k - k_0) \left\{ [2M \beta_0^2 - N \alpha_1 \beta_0 - (M^2 + N^2) (\beta_0^2 + \frac{\alpha_1^2}{4})] k \right. \\ & \left. + (M^2 + N^2 - M) (\beta_0^2 + \frac{\alpha_1^2}{4}) k_0 \right\} . \end{aligned} \quad (3.46)$$



A comparison of Eq. (3.45) with Eq. (3.46) allows us to compute the time-average of the lost power (i.e., the wasted power) due to the kinetic energy in the wake.

$$\overline{C_W} = \overline{C_P} - \overline{C_{F-\text{with wake}}} = \frac{1}{2}(k - k_0)^2(M - M^2 - N^2)(\beta_0^2 + \frac{\alpha_1^2}{4}) . \quad (3.47)$$

This lost power in Eq. (3.47) can alternatively be expressed in terms of the original flow variables,

$$\begin{aligned} \overline{C_W} &= (w_0 + \frac{1}{2}w_2 - \lambda_0)\lambda_0 \\ &= (\dot{h}_0 + \frac{1}{2}\dot{h}_1 + \sum_{n=1}^{\infty} nh_n - \lambda_0)\lambda_0 . \end{aligned} \quad (3.48)$$

The combinator  $M - M^2 + N^2$  is plotted in Fig. 3.2. Note that it is monotonically increasing with  $k$  and is always positive, reaching a maximum of 0.25 at  $k = \infty$ . One can see from Eq. (3.47) and Fig. 3.2 that the wasted power is always positive and is proportional both to  $(k - k_0)^2$  and to the input motion,  $[\beta_0^2 + \alpha_1^2/4]$ . Thus, for the case  $k < k_0$  which corresponds to negative  $\overline{C_F}$  (power required to pull the airfoil) and negative  $\overline{C_P}$  (power extracted from the free-stream to deform the airfoil), these losses lower the absolute value of the extracted energy. For  $k > k_0$  which corresponds to positive  $\overline{C_F}$  (propulsive power on the airfoil), these losses decrease the useful propulsive power.

From the above development, we can look at the efficiency of the flexible wing either as a propulsive device ( $k > k_0$ ) or as an energy extraction device ( $k < k_0$ ). For  $k > k_0$ , the case of propulsion, the efficiency is defined as the propulsive efficiency—the power providing propulsion ( $\overline{C_F}$ ) divided by the total power put into the system by the airfoil ( $\overline{C_P}$ ). For  $k < k_0$ , which is the case of energy extraction, the efficiency is defined as the total power extracted from the flow ( $\overline{C_P}$ ) divided by the total power required to drive the airfoil through the flow ( $\overline{C_F}$ ). Note that this is exactly the reciprocal of the propulsive efficiency. Thus, we may write the general efficiency  $\epsilon$  as

$$\begin{aligned} \epsilon &= \overline{C_F}/\overline{C_P} = 1 - \overline{C_W}/\overline{C_P} , \quad (k > k_0), \\ \epsilon &= \overline{C_P}/\overline{C_F} = 1 - \overline{C_W}/\overline{C_F} , \quad (k < k_0). \end{aligned} \quad (3.49)$$

Thus, the energy lost into the wake  $\overline{C_W}$  always subtracts from the efficiency.

### 3.4 Numerical Results

In this section, we present numerical results for force coefficients. Results are given both in the time-domain and in terms of the time-averaged coefficients. We use the parameters of *C. elegans* swimming in 5wt% PVP aqueous solution as references. From Table 2.2, the average normalized wavelength of swimming *C. elegans* in the least viscous testing fluid (5PVP) is 0.87, the average normalized amplitude is 0.17, the average frequency is 1.71 Hz, and the normalized moving speed is 0.25 1/s. Also, the average normalized wavelength of crawling *C. elegans* is 0.62 [10]. For comparison, we choose these parameters as references in our calculation, that is,  $A/b = 0.2$ ,  $z = \Lambda/(2b) = 0.6, 0.9$ ,  $f = 1.71$  Hz, and  $u_0/(2b) = 0.25$ . For convenience, we normalized the parameters with the chord length  $2b$  instead of body length  $L$ . If the amplitude is small enough,  $2b \approx L$ .

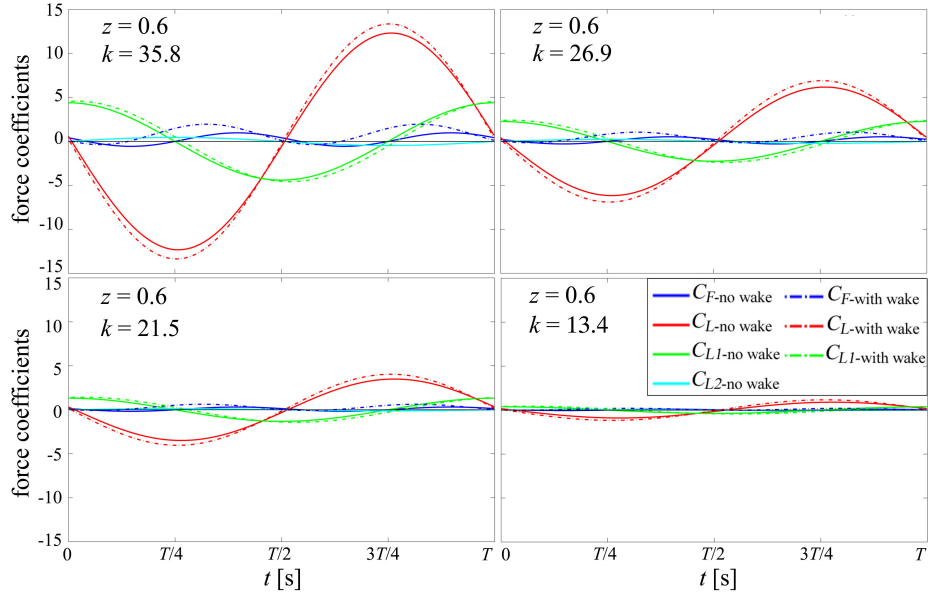


Figure 3.3: The time-dependent coefficients of all forces (with and without shed vorticity effects) for one undulatory period  $T$ , at  $A/b = 0.2$  and  $z = 0.6$  and four different reduced frequencies.

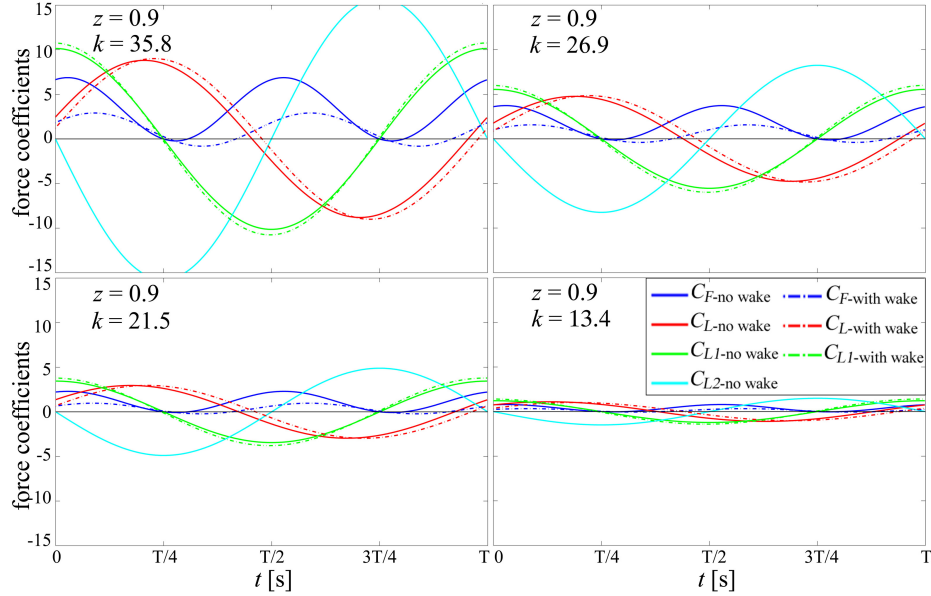


Figure 3.4: The time-dependent coefficients of all forces (with and without shed vorticity effects) for one undulatory period  $T$ , at  $A/b = 0.2$  and  $z = 0.9$  and four different reduced frequencies.

Figure 3.3 and 3.4 present results in the time domain for all force coefficients at four different reduced frequencies,  $k = 35.8$ ,  $k = 26.9$ ,  $k = 21.5$ , and  $k = 13.4$ . Figure 3.3 are results for  $z = 0.6$  and Fig. 3.4 are results for  $z = 0.9$ . Results are presented both with and without wake effects over one period  $T$  of undulation. Three different loading coefficients are given.  $C_L$  is the lift coefficient,  $C_{L1}$  is the coefficient of pitching moment, and  $C_{L2}$  is the coefficient of camber force. Note that each loading coefficient goes through one oscillation with zero mean, while the propulsive force goes through two oscillations—with a mean no greater than the amplitude. Two things are noteworthy from these plots regardless of the  $z$  value. First, all loads decrease as  $k$  approaches  $k_0 = \pi/z$ . When  $k = k_0$ , all forces are zero (not shown). Second, the effect of induced flow has more impact on the propulsive coefficient than other coefficients. The results that has shed vorticity effect are shown in dash lines. As it is expected, the induced flow increases the fluctuation of loading coefficients. Interestingly, the induced flow increases the mean and the amplitude of propulsive coefficient at  $z = 0.6$ , but reduces the mean and the amplitude of propulsive coefficient at  $z = 0.9$ .

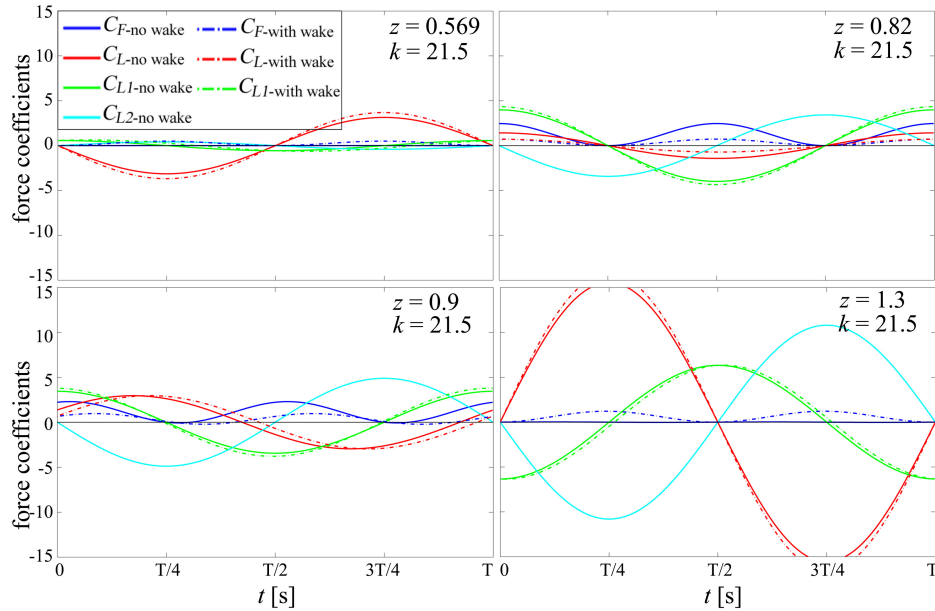


Figure 3.5: The time-dependent coefficients of all forces (with and without shed vorticity effects) for one undulatory period  $T$ , at  $A/b = 0.2$  and  $k = 21.5$  and four different wavelength  $z$ . At  $z = 0.569$  and  $z = 1.3$ ,  $\beta_0 = 0$ . At  $z = 0.82$ ,  $\alpha_1 = 0$  and  $\beta_0$  is at its region extrema.

Now we look at these force coefficients at four different wavelengths,  $z = 0.569$ ,  $0.82$ ,  $0.9$ , and  $1.3$ , as shown in Fig. 3.5. The results are shown for  $k = 21.5$  (typical of swimming *C. elegans* in 5PVP). Since  $z$  changes the critical reduced frequency  $k_0$ , it also changes the phasing of the lift loads. At  $z = 0.569$  and  $z = 1.3$ ,  $\beta_0 = 0$ . If there were no shed vorticity, the propulsive force is zero. With the existence of shed vorticity, a positive propulsive force is generated by the input of  $\alpha_1$ . However, the system will require more power to compensate the impact of induced flow in moving the wing. As seen in these plots, the amplitudes of all loading forces are significant, especially for  $z = 1.3$ . This implies the instability of the motion. On the other hand, at  $z = 0.82$ ,  $\alpha_1 = 0$  and  $\beta_0$  is at its regional extrema ( $J_0' = -J_1$ ). For the case of no shed vorticity, the motion could obtain the highest propulsive force at fixed  $k$ . The shed vortices will hold the wing back and reduce the propulsive force. Figures 3.3, 3.4 and 3.5 each verifies that our formulas for mean and oscillatory loads are correct.

Figure 3.6 and 3.7 then present the time-averaged propulsive coefficients with and without wake versus reduced frequency for  $z = 0.6$  and  $z = 0.9$ . By plotting versus

$k/(k+1)$ , we effectively show all reduced frequencies from zero to infinity on the same plot. The left plot shows the entire range, while the right plot focuses on the region of positive propulsive force. When divided by  $k(k+1)$ , Eq.3.37 becomes  $\overline{C_{F-\text{no wake}}}/[k(k+1)] = a_1X + a_2(1-X)$ , where  $X = k/(k+1)$ ,  $a_1 = \beta_0^2/2$  and  $a_2 = -k_0\beta_0^2/2$ . When  $k = 0$ ,  $X = 0$ , and  $\overline{C_{F-\text{no wake}}}$  is  $a_2$ ; as  $k$  goes to infinity,  $X = 1$ , and  $\overline{C_{F-\text{no wake}}}$  will be  $a_1$ . Therefore, the plots with no induced flow are straight lines in this normalized space while curves with induced flow. This is because  $M(k)$  and  $N(k)$  vary in a nonlinear fashion as shown in Fig. 3.2. For  $k > k_0$ , the time-averaged propulsive coefficient is always positive with or without wake effects. At  $z = -0.6$  (Fig. 3.6), the wing will gain a larger propulsion with the existence of shed vortices; at  $z = 0.9$  (Fig. 3.6), the shed vorticity reduces the propulsive coefficient. This is a result of the value of the Bessel functions in  $\beta_0$  and  $\alpha_1$  at different  $z$ . For  $k < k_0$ , the propulsive force become drag, and the shed vorticity become the main contributor to the drag force as  $k$  goes to zero.

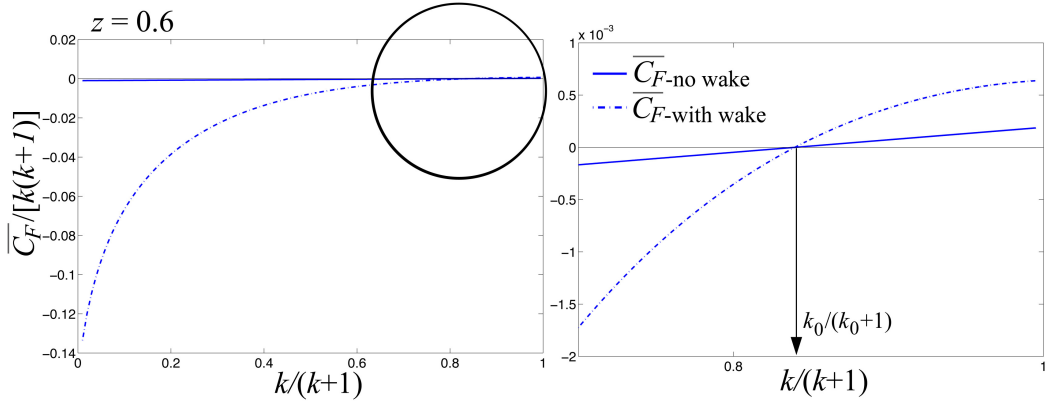


Figure 3.6: Normalized time-averaged propulsive coefficient (with and without shed wake) versus scaled reduced frequency  $k/(k+1)$  at  $A/b = 0.2$  and  $z = 0.6$  ( $k_0/(k_0+1) \approx 0.84$ ). The right plot is an enlarged view of the circle in the left plot.

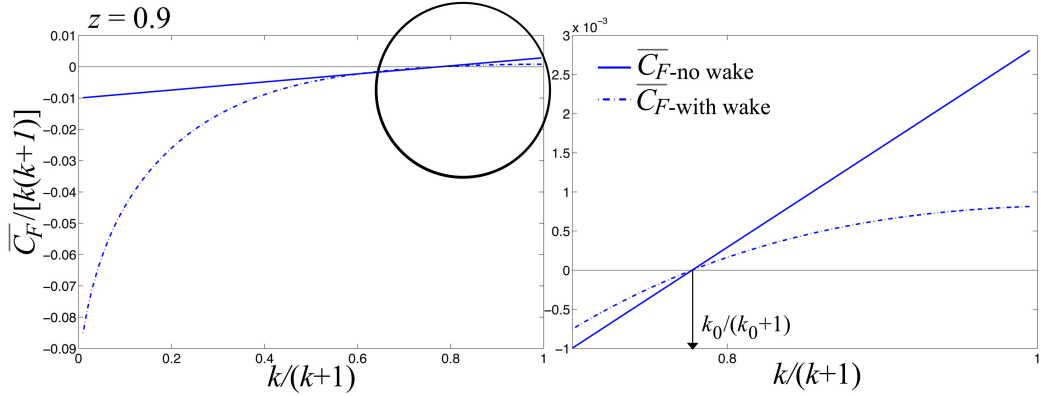


Figure 3.7: Normalized time-averaged propulsive coefficient (with and without shed wake) versus scaled reduced frequency  $k/(k+1)$  at  $A/b = 0.2$  and  $z = 0.9$  ( $k_0/(k_0+1) \approx 0.78$ ). The right plot is an enlarged view of the circle in the left plot.

Figure 3.8 shows the time-averaged propulsive coefficients with and without wake as functions of  $k_0$  (i.e., of  $\pi/z$ ) at given values of  $k = 23.56$  and  $k = 11.78$ . Without wake, one can see the oscillatory effect of  $k_0$  due to the Bessel functions in  $\beta_0$  and  $\alpha_1$ . When  $J_0(k_0)$  is zero,  $J_1(k_0)$  is very close to its extreme; when  $J_1$  is zero,  $J_0$  is at its extreme ( $J'_0 = -J_1$ ). Thus, the peaks in Fig. 3.8 are at the maxima of  $J_0$  ( $J_1 = 0$  and all  $\beta_0$ ), and the minima are when  $J_0 = 0$  (all  $\alpha_1$ ). Because the regional peaks of  $J_0$  decrease with  $k_0$ , the the regional peaks of  $\overline{C_F}$  decrease with  $k_0$  for the case of no inflow. With inflow, the peaks are smoothed out because  $\lambda_0$  couples the lift through phase shift. Nonetheless, the propulsive force still diminished with  $k_0$ . Particularly, at  $z = 0.569$  and  $z = 1.3$  the propulsive force of no wake effect is zero and the wake alone contributes to the propulsion. At the case of no shed vorticity, the optimum propulsion is at  $z = 0.82$  ( $k_0 = 3.83$ ). Interestingly, *C. elegans* has an average normalized wavelength of 0.62 for crawling (no propulsive force needed), while it uses an average normalized wavelength of 0.88 for swimming (more propulsive force required). Though, the shed vorticity may increase or reduce the the propulsive force, it always consumes part of the total power for the motion.

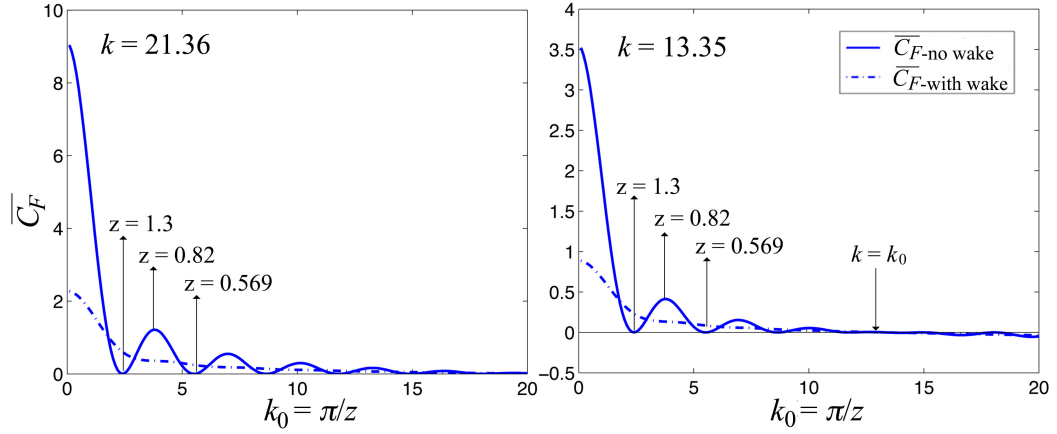


Figure 3.8: The time-averaged propulsive coefficient (with and without shed wake) versus critical reduced frequency  $k_0 = \pi/z$  at  $A/b = 0.2$ . The left plot is at  $k = 21.36$ , and the right one is at  $k = 13.35$ . The peaks of time averaged propulsion only depend on  $k_0$  (or  $z$ ).

Figure 3.9 shows the the power required for wing motion, the propulsive power, and the lost power due to wake versus the quantity  $k/(k + 1)$  for  $A/b = 0.2$  and  $z = 0.9$ . (Each power is normalized by  $k(k + 1)$  to facilitate the comparison.) One can see the lost power due to wake is always positive. For  $k < k_0$ , the power extracted from the free-stream (the absolute value of  $\overline{C_F}$ ) is diminished by wake losses; and, for  $k > k_0$ , the power required for propulsion  $\overline{C_P}$  is reduced by wake losses. As  $k$  goes infinity, the shed vorticity will consume up to 50% of the total power input.

We also look at how the change of wavelength will affect the powers for fixed  $k$ . As shown in Fig. 3.10,  $A/b = 0.2$  and  $k = 13.35$ . First,  $z$  has to be large enough that  $k_0 = \pi/z$  will be smaller than  $k$  to obtain a positive propulsion. Second, as  $z$  becomes large, that is,  $k_0$  approaching to zero, the system requires more power input and less percentage of total power will be used for propulsion. At a special care of  $z = \infty$  ( $k_0 = 0$ ), only half of the total power input will be used for propulsion while the other half will be consumed by the wake. Third, for  $k_0 < k$ , the curve can be divided into two sections of different slopes. For large  $z$  (small  $k_0$ ), the slope of powers verse  $k_0$  is much steeper. The transition between the two sections is around  $k_0 = 3$  ( $z \approx 1$ ).

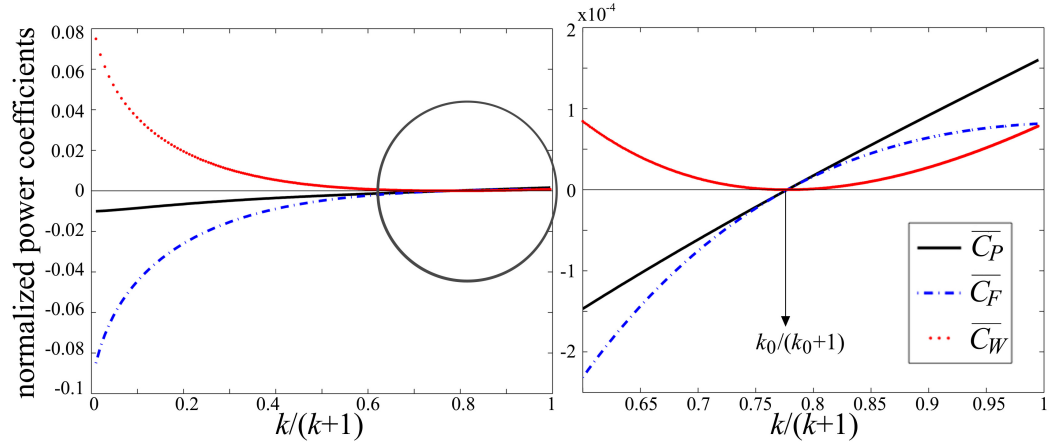


Figure 3.9: Time-averaged power coefficients normalized to  $k(k+1)$  versus  $k/(k+1)$ , at  $A/b = 0.2$  and  $z = 0.9$  (or  $k_0 = 3.49$ ).  $\overline{C_P}$  is the power required for wing motion,  $\overline{C_F}$  is propulsive power with wake effects, and  $\overline{C_W}$  is the lost power due to wake. The plot on the right is an enlarged view of the circle in the left plot.

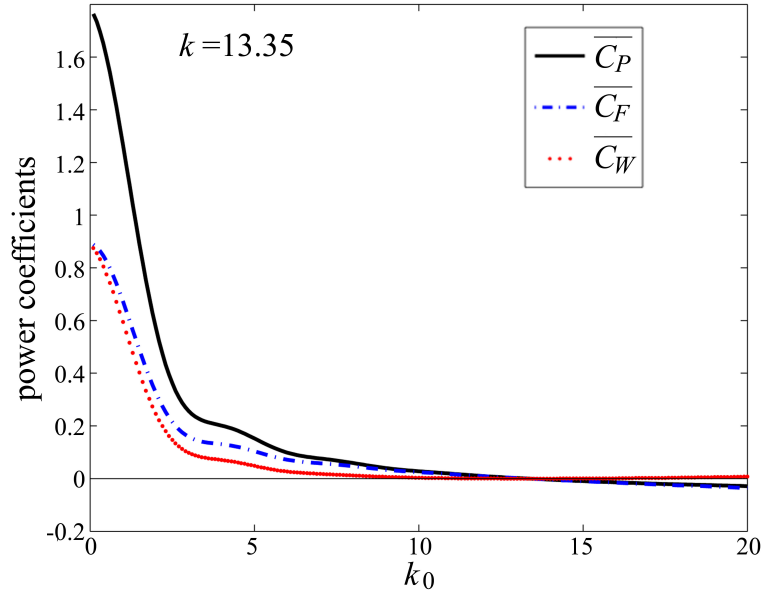


Figure 3.10: The time-averaged power coefficients verse critical reduced frequency  $k_0$ , for  $A/b = 0.2$ ,  $k = 13.36$ .  $\overline{C_P}$  is the power required for wing motion,  $\overline{C_F}$  is propulsive power with wake effects, and  $\overline{C_W}$  is the lost power due to wake.



Figure 3.11 shows the efficiency of a flexible wing (including wake effects) as either a propulsive device or an energy extraction device, based on Eq. (3.49). In the left-hand panel of the figure, the critical frequency is taken as  $k_0 = 3.83$ . For the case of a propulsive device,  $k > k_0$ , it is useful to plot power versus the normalized quantity  $(k - k_0)/(k + k_0)$  as is done. The propulsive efficiency decreases from 1.0 to 0.5 as the reduced frequency increases beyond  $k_0$  and approaches infinity. This implies that, at the beginning of the sinusoidal motion from rest (small  $u_0$ ), the propulsive efficiency will be 0.5, but the propulsive efficiency will increase as  $u_0$  becomes larger (and  $k$  becomes smaller). The right-hand panel of Fig. 3.11 plots the efficiency  $\epsilon$  versus  $k_0$  for a fixed value of  $k = 11.78$ . The part of the curve with  $k_0 < k$  is the case of propulsion. As in the right-hand panel, it varies from 0.5 to 1.0. The part of the curve with  $k_0 > k$  is for an energy extraction device, and the efficiency continuously drops as  $k_0$  is increased.

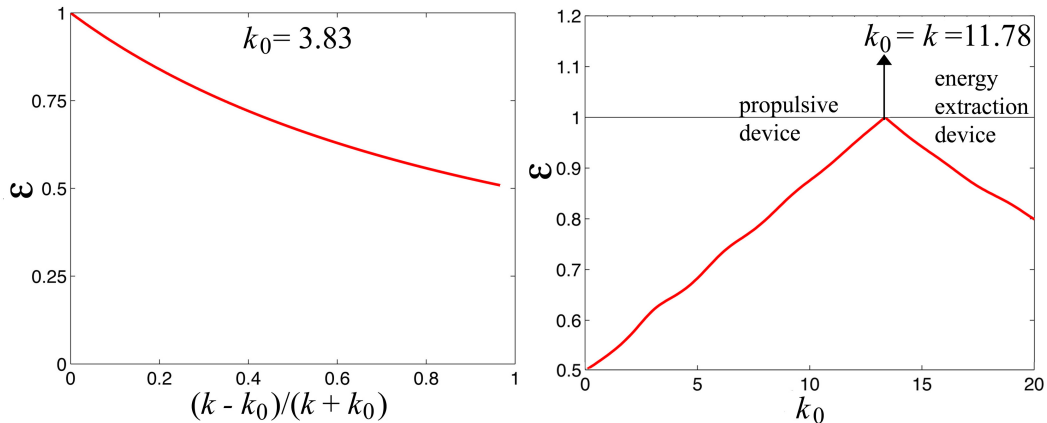


Figure 3.11: The propulsive efficiency  $\epsilon$  verse  $(k - k_0)/(k + k_0)$  (left) and  $k_0$  (right). The left plot only shows when  $k > k_0$ , that is  $(k - k_0)/(k + k_0) > 0$  for  $A/b = 0.2$  and  $z = 0.9$ . The right plot shows the results for  $k = 11.78$ .

To obtain a high propulsive efficiency, the system has to operate at a small wavelength  $z$  (large  $k_0$ ), but this also results in small propulsive power as shown in Fig. 3.10. Thus,  $z \approx 0.87$ , which is the average wavelength of swimming *C. elegans*, seems a very reasonable wavelength that the system does not need too much power to operate and has a relatively high efficiency.

### 3.5 Summary

The propulsive force, lift and generalized forces of sinusoidal locomotion are presented as dimensionless coefficients (normalized by  $2\pi\rho b u_0^2$ ).

The coefficient of propulsion  $C_{F\text{-with wake}} = C_{F\text{-no wake}} - \Delta C_F$ , and

$$C_{F\text{-no wake}} = (k - k_0)k\beta_0 \left[ \beta_0 \cos^2(k\tau) + \frac{\alpha_1}{2} \cos(k\tau) \sin(k\tau) \right], \quad (3.50)$$

$$\begin{aligned} \Delta C_F = & (k - k_0) \left\{ [(2\lambda_\alpha\beta_0 - \lambda_\alpha^2)k - (\lambda_\alpha^2 - \lambda_\alpha\beta_0)k_0] \cos^2(k\tau) \right. \\ & + [(2\lambda_\beta\beta_0 - 2\lambda_\alpha\lambda_\beta)k - (\lambda_\beta\beta_0 - \frac{1}{2}\lambda_\alpha\alpha_1 + 2\lambda_\alpha\lambda_\beta)k_0] \cos(k\tau) \sin(k\tau) \\ & \left. + [-\lambda_\beta^2k + (\frac{1}{2}\lambda_\beta\alpha_1 + \lambda_\beta^2)k_0] \sin^2(k\tau) \right\}. \end{aligned} \quad (3.51)$$

The coefficient of lift  $C_{L\text{-with wake}} = C_{L\text{-no wake}} - \Delta C_L$ , and

$$C_{L\text{-no wake}} = -(k - k_0) \left[ \beta_0 \cos(k\tau) + \frac{\alpha_1}{2k_0} (k - k_0) \sin(k\tau) \right], \quad (3.52)$$

$$\Delta C_L = -(k - k_0)[\lambda_\alpha \cos(k\tau) + \lambda_\beta \sin(k\tau)]. \quad (3.53)$$

The coefficient of pitching moment  $C_{L1\text{-with wake}} = C_{L1\text{-no wake}} - \Delta C_{L1}$ , and

$$C_{L1\text{-no wake}} = \frac{(k - k_0)}{2k_0} \left[ \left( \frac{\alpha_1}{k_0} - \beta_0 \right) k - \alpha_1 \right] \cos(k\tau),$$

$$\Delta C_{L1} = \frac{1}{2}(k - k_0)[\lambda_\alpha \cos(k\tau) + \lambda_\beta \sin(k\tau)].$$

The coefficient of bending moment  $C_{L2\text{-with wake}} = C_{L2\text{-no wake}} - \Delta C_{L2}$ , and

$$C_{L2\text{-no wake}} = 2 \frac{(k - k_0)^2}{k_0^2} \left( \frac{\alpha_1}{k_0} + \beta_0 \right) \sin(k\tau). \quad (3.54)$$

$$\Delta C_{L2} = 0. \quad (3.55)$$

Where,  $k = \omega b/u_0$  the reduced frequency,  $\tau = u_0 t/b$  the reduced time,  $k_0 = \pi/z$ ,  $\beta_0 = (A/b)J_0(k_0)$ ,  $\alpha_1 = (2A/b)J_1(k_0)$ ,  $\lambda_\alpha = M\beta_0 - N\alpha_1/2$ , and  $\lambda_\beta = -M\alpha_1/2 - N\beta_0$ .  $M$  and  $N$  are approximated as the following functions of  $X = k/(k+1)$ ,

$$M(X) = 0.5 - 0.5(1-X)^4 - 0.1X(1-X)^2 - 0.152X(1-X)^3 + 0.47X(1-X)^4, \quad (3.56)$$

$$N(X) = -X \ln(X)(1-X)^3 + 0.0905X(1-X) + 0.609X(1-X)^2 - 0.686X(1-X)^3. \quad (3.57)$$

The time-averaged lift and generalized forces are zero. The time-averaged coefficient of propulsion  $\overline{C_{F-\text{with wake}}} = \overline{C_{F-\text{no wake}}} - \Delta\overline{C_F}$  is

$$\overline{C_{F-\text{no wake}}} = \frac{1}{2}k(k-k_0)\beta_0^2, \quad (3.58)$$

$$\begin{aligned} \Delta\overline{C_F} = & \frac{k-k_0}{2} \left\{ [2M\beta_0^2 - N\alpha_1\beta_0 - (M^2 + N^2)(\beta_0^2 + \frac{\alpha_1^2}{4})]k \right. \\ & \left. + (M^2 + N^2 - M)(\beta_0^2 + \frac{\alpha_1^2}{4})k_0 \right\}. \end{aligned} \quad (3.59)$$

The time-averaged coefficient of propulsive power is

$$\begin{aligned} \overline{C_P} = & \frac{1}{2}k(k-k_0)\beta_0^2 - \frac{1}{2}(k-k_0) \left\{ [2M\beta_0^2 - N\alpha_1\beta_0 - (M^2 + N^2)(\beta_0^2 + \frac{\alpha_1^2}{4})]k \right. \\ & \left. + (M^2 + N^2 - M)(\beta_0^2 + \frac{\alpha_1^2}{4})k_0 \right\}. \end{aligned} \quad (3.60)$$

The time-averaged coefficient power required for the wing to performing the sinusoidal motion is

$$\overline{C_P} = \frac{1}{2}k(k-k_0)\beta_0^2 - \frac{1}{2}k(k-k_0)(M\beta_0^2 - M\frac{\alpha_1^2}{4} - N\alpha_1\beta_0). \quad (3.61)$$

The time-averaged coefficient of power lost in wake is

$$\overline{C_W} = \overline{C_P} - \overline{C_{F-\text{with wake}}} = \frac{1}{2}(k-k_0)^2(M - M^2 - N^2)(\beta_0^2 + \frac{\alpha_1^2}{4}). \quad (3.62)$$

# Chapter 4

## Discussion

While the resistive force theory is derived for a steady propulsion when the propulsive force is zero, our results can explain how a sinusoidal locomotion starts from the initially still state. When a wing starts to wrap at a certain frequency  $f$ , the reduced frequency  $k = \omega b/u_0$  is very high because the moving speed  $u_0$  is very small, which gives the wing a high propulsion. As the wing accelerates,  $u_0$  becomes larger and  $k$  becomes smaller (for fixed frequencies  $f$ ), which produces less propulsive force. If the system requires additional propulsive force, the wing need to increase the undulatory frequency  $f$ . This is common in nature when birds have to flap more to begin flight. If the viscous force is negligible (at high Reynolds numbers), then when  $u_0/(2b)$  eventually reaches the wave speed  $fz$ , that is when  $k = k_0 = \pi/z$ , the propulsive force becomes zero which enables the system to keep moving at the speed of  $u_0/(2b) = fz$ . For viscous flows (small Reynolds numbers), the moving speed can not reach to the wave speed because the propulsion from the potential flow is used to compensate for the drag due to viscosity.

On the other hand, the cost of a high reduced frequency is the increase of the fluctuation of all forces. At certain moments, there will be negative propulsive force, which means the object might temporarily go backwards even though the time-averaged propulsion is positive. We observed that swimming *C. elegans* slipped twice in the moving direction over one undulatory period as shown in Fig. 4.1. Moreover, for  $k > k_0$ , the lift, pitching moment and bending moment are fluctuating with time. The whole object will therefore move up and down, tilt to left and right, and bear certain bending moment over one undulation period. This can explain the  $y$ -axis

direction deviation of *C. elegans* we observed in Chapter 2 when it is in less viscous fluids.

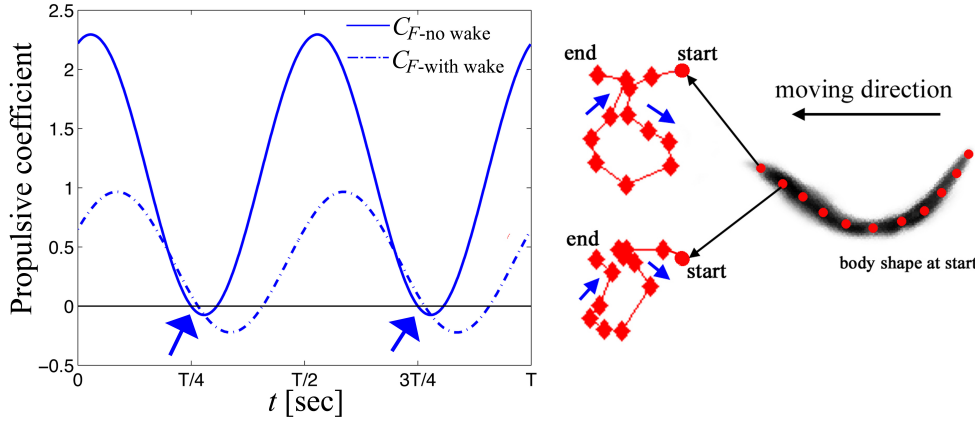


Figure 4.1: Both the state-space airloads theory and the experiments show back slips of sinusoidal locomotion over one period under certain condition. Blue arrows point out the negative propulsive force and slips.

The effects of shed vorticity are very important. First, the shed vortices can increase or reduce the time-averaged propulsive force for  $k > k_0$ . This depends on the phasing of the inflow due to the shed wake. By adjusting the wavelength of the sinusoidal motion, the wing can move around the shed vortices, and these vortices only apply normal force on the wing surface which promote the propulsion. Similarly, at certain wavelengths, the wing can undulate in a way in which there is only longitudinal force on the wing, which become drag. Second, however, the shed vorticity smoothes the effect of wavelength on the propulsive force at a fixed  $k$ . Without shed vorticity effects, from  $z = 0.569$  to  $1.3$ , the time-averaged propulsion will go through 3 extrema (shown in Fig. 3.8). This might cause great instability even if the wing slightly changes the wavelength during the movement. In reality, the transition of time-averaged propulsion respect to the wavelength should be as smooth as expected with the existence of shed vortices. Last, though the shed wake might contribute to the propulsive force, it always detracts power from the total power input to the system, giving a propulsive efficiency between 0.5 to 1.0. The ideal case of 1.0 propulsive efficiency is at  $k = k_0$  when there is no shed vorticity. Both high reduced frequency  $k$  and large wavelength  $z$  will lead to a small efficiency with the limit of 0.5.

# Chapter 5

## Conclusions

In this work, we quantitatively studied the locomotory gaits of swimming *C. elegans* in Newtonian and non-Newtonian fluids. Numerical analysis of the videos of swimming *C. elegans* shows that its locomotion can be predicted by a sinusoidal function with certain degrees of slippage. The statistic results of its locomotory gaits show that fluid viscosity will reduce the undulatory frequency but not the velocity, while fluid elasticity will reduce the velocity but not the frequency. However, the wavelength of swimming *C. elegans* remains the same and is greater than the wavelength for crawling. According to the resistive force theory, we found the ratio of resistive coefficients  $C_n/C_l$  gets smaller for more elastic fluids.

For the cases of high Reynolds numbers, we applied the state-space airloads theory to the sinusoidal locomotion of a thin flexible wing in two dimensions. We have derived the closed forms of propulsive force, lift, pitching moment and bending moment as functions of time. We also gave the equations of the time-average propulsive force, the power required to perform the sinusoidal motion, the power used for propulsion, and the power lost due to wake. Our result shows that at a reduced frequency  $k$  higher than  $k_0 = \pi/z$ , a flexible wing can obtain a positive time-averaged propulsion by performing sinusoidal motion. As  $k$  reduces to  $k_0$ , the system approaches an ideal steady state with efficiency of 1.0. Wavelength of the sinusoidal motion plays an important role. It can greatly affect the time-averaged propulsion if there is no shed vorticity, that at  $z = 0.569$  and  $z = 1.3$  there is no propulsive force; at  $z = 0.82$ , the system can gain the optimal propulsion. It also affects the total power required to perform the sinusoidal motion and the propulsive efficiency. The average wavelength of swimming *C. elegans*  $z \approx 0.9$  seems a very reasonable that the system does not

require too much power input and can move at a relatively high propulsive efficiency. According to our results, the lowest propulsive efficiency of the sinusoidal propulsion ( $k > k_0$ ) is 0.5, which still can be considered efficient.

# Appendix A

## Proofs of Certain Identities Involving Bessel Functions

Here we are going to show the derivations of following identities,

$$\sum_{n=1}^{\infty} n\alpha_n = -k_0\beta_0 , \quad (\text{A.1})$$

$$\sum_{n=1}^{\infty} n\beta_n = \frac{1}{2}k_0\alpha_1 , \quad (\text{A.2})$$

$$\sum_{n=1}^{\infty} n(\alpha_n^2 - \beta_n^2) = -k_0\alpha_1\beta_0 , \quad (\text{A.3})$$

$$\sum_{n=1}^{\infty} n\alpha_n\beta_n = 0 , \quad (\text{A.4})$$

where  $k_0 = \pi/z$ .

The values of  $\alpha_n$  and  $\beta_n$  are

$$\begin{aligned} \alpha_0 &= 0 , & \beta_0 &= \frac{A}{b}J_0(k_0) , \\ \alpha_n &= -\frac{2A}{b}\sin\left(\frac{n\pi}{2}\right)J_n(k_0) , & \beta_n &= \frac{2A}{b}\cos\left(\frac{n\pi}{2}\right)J_n(k_0) , \quad (n \geq 1) . \end{aligned} \quad (\text{A.5})$$



Definition of Bessel functions of the first kind with integer argument  $n$  [4] is

$$J_n(x) = \sum_{m=0}^{\infty} \frac{-1^m}{m!(m+n)!} \left(\frac{x}{2}\right)^{2m+n} . \quad (\text{A.6})$$

One of the identities of Bessel functions of the first kind we will use is

$$J_n(x) = \frac{x}{2n} [J_{n-1}(x) + J_{n+1}(x)] . \quad (\text{A.7})$$

Therefore,

$$\begin{aligned} \sum_{n=1}^{\infty} n\alpha_n &= -\frac{2A}{b} \sum_{n=1}^{\infty} n \sin\left(\frac{n\pi}{2}\right) J_n(k_0) \\ &= -\frac{2A}{b} \sum_{n=1}^{\infty} n \sin\left(\frac{n\pi}{2}\right) \frac{k_0}{2n} [J_{n-1}(k_0) + J_{n+1}(k_0)] \\ &= -\frac{A}{b} k_0 \left[ \sum_{n=1}^{\infty} \sin\left(\frac{n\pi}{2}\right) J_{n-1}(k_0) + \sum_{n=1}^{\infty} \sin\left(\frac{n\pi}{2}\right) J_{n+1}(k_0) \right] \\ &= -\frac{A}{b} k_0 \left\{ \sum_{n=0}^{\infty} \sin\left[\frac{(n+1)\pi}{2}\right] J_n(k_0) + \sum_{n=2}^{\infty} \sin\left[\frac{(n-1)\pi}{2}\right] J_n(k_0) \right\} \\ &= -\frac{A}{b} k_0 \left[ \sum_{n=0}^{\infty} \cos\left(\frac{n\pi}{2}\right) J_n(k_0) - \sum_{n=2}^{\infty} \cos\left(\frac{n\pi}{2}\right) J_n(k_0) \right] \\ &= -\frac{A}{b} k_0 J_0(k_0) \\ &= -k_0 \beta_0 . \end{aligned} \quad (\text{A.8})$$

Similarly,

$$\begin{aligned}
\sum_{n=1}^{\infty} n\beta_n &= \frac{2A}{b} \sum_{n=1}^{\infty} n \cos\left(\frac{n\pi}{2}\right) J_n(k_0) \\
&= \frac{2A}{b} \sum_{n=1}^{\infty} n \cos\left(\frac{n\pi}{2}\right) \frac{k_0}{2n} [J_{n-1}(k_0) + J_{n+1}(k_0)] \\
&= \frac{A}{b} k_0 \left[ \sum_{n=1}^{\infty} \cos\left(\frac{n\pi}{2}\right) J_{n-1}(k_0) + \sum_{n=1}^{\infty} \cos\left(\frac{n\pi}{2}\right) J_{n+1}(k_0) \right] \\
&= \frac{A}{b} k_0 \left\{ \sum_{n=0}^{\infty} \cos\left[\frac{(n+1)\pi}{2}\right] J_n(k_0) + \sum_{n=2}^{\infty} \cos\left[\frac{(n-1)\pi}{2}\right] J_n(k_0) \right\} \\
&= \frac{A}{b} k_0 \left[ - \sum_{n=0}^{\infty} \sin\left(\frac{n\pi}{2}\right) J_n(k_0) + \sum_{n=2}^{\infty} \sin\left(\frac{n\pi}{2}\right) J_n(k_0) \right] \\
&= -\frac{A}{b} k_0 J_1(k_0) \\
&= \frac{k_0}{2} \alpha_1 .
\end{aligned} \tag{A.9}$$

$$\begin{aligned}
\sum_{n=1}^{\infty} n(\alpha_n^2 - \beta_n^2) &= \left(\frac{2A}{b}\right)^2 \sum_{n=1}^{\infty} n \left[ \sin^2\left(\frac{n\pi}{2}\right) - \cos^2\left(\frac{n\pi}{2}\right) \right] J_n^2(k_0) \\
&= \left(\frac{2A}{b}\right)^2 \sum_{n=1}^{\infty} n [-\cos(n\pi)] J_n^2(k_0) \\
&= -\left(\frac{2A}{b}\right)^2 \sum_{n=1}^{\infty} (-1)^n n J_n^2(k_0) \\
&= -\left(\frac{2A}{b}\right)^2 \sum_{n=1}^{\infty} (-1)^n n \frac{k_0}{2n} [J_{n-1}(k_0) + J_{n+1}(k_0)] J_n(k_0) \\
&= -\left(\frac{2A}{b}\right)^2 \frac{k_0}{2} \left[ \sum_{n=1}^{\infty} (-1)^n J_{n-1}(k_0) J_n(k_0) + \sum_{n=1}^{\infty} (-1)^n J_n(k_0) J_{n+1}(k_0) \right] \\
&= -\left(\frac{2A}{b}\right)^2 \frac{k_0}{2} \left[ \sum_{n=0}^{\infty} (-1)^{n+1} J_n(k_0) J_{n+1}(k_0) + \sum_{n=1}^{\infty} (-1)^n J_n(k_0) J_{n+1}(k_0) \right] \\
&= -\left(\frac{2A}{b}\right)^2 \frac{k_0}{2} \left[ -\sum_{n=0}^{\infty} (-1)^n J_n(k_0) J_{n+1}(k_0) + \sum_{n=1}^{\infty} (-1)^n J_n(k_0) J_{n+1}(k_0) \right] \\
&= \left(\frac{2A}{b}\right)^2 \frac{k_0}{2} J_0(k_0) J_1(k_0) \\
&= -k_0 \alpha_1 \beta_0 \tag{A.10}
\end{aligned}$$

$$\begin{aligned}
\sum_{n=1}^{\infty} n \alpha_n \beta_n &= -\left(\frac{2A}{b}\right)^2 \sum_{n=1}^{\infty} n \sin\left(\frac{n\pi}{2}\right) \cos\left(\frac{n\pi}{2}\right) J_n^2(k_0) \\
&= -\left(\frac{2A}{b}\right)^2 \sum_{n=1}^{\infty} n \frac{\sin(n\pi)}{2} J_n^2(k_0) \\
&= 0 . \tag{A.11}
\end{aligned}$$

# References

- [1] A. Afonso, M. A. Alves, F. T. Pinho, and P. J. Oliveira. Uniform flow of viscoelastic fluids past a confined falling cylinder. *Rheologica Acta*, 47(3):325–348, 2008.
- [2] D. L. Altshuler, W. B. Dickson, J. T. Vance, S. P. Roberts, and M. H. Dickinson. Short-amplitude high-frequency wing strokes determine the aerodynamics of honeybee flight. *Proceedings of the National Academy of Sciences of the United States of America*, 102(50):18213–18218, 1999.
- [3] G. N. Cox, M. Kusch, and R. S. Edgar. Cuticle of *Caenorhabditis elegans*. *The Journal of Cell Biology*, 90:7–17, 1981.
- [4] I. S. Gradshteyn and I. M. Ryzhik. *Table of integrals, Series and Products*. Academy Press, San Diego, CA, sixth edition, 2000.
- [5] J. Gray and G. J. Hancock. The propulsion of sea-urchin spermatozoa. *The Journal of Experimental Biology*, 32:802–814, 1955.
- [6] J. Gray and H. W. Lissmann. The locomotion of nematodes. *The Journal of Experimental Biology*, 41:135–154, 1964.
- [7] G. J. Hancock. The self-propulsion of microscopic organisms through liquids. *Proceedings of the Royal Society of London*, 217(1128):96–121, 1953.
- [8] D. F. James. Boger fluids. *Annual Review of Fluid Mechanics*, 41:129–142, January 2009.
- [9] R. E. Johnson. *Slender-body theory for stokes flow and flagellar hydrodynamics*. PhD thesis, California Institute of Technology, 1977.
- [10] J. Karbowski, C. J. Cronin, A. Seah, J. E. Mendel, D. Cleary, and P. W. Sternberg. Conservation rules, their breakdown and optimality in *Caenorhabditis* sinusoidal locomotion. *The Journal of Theoretical Biology*, 242:652–669, 2006.
- [11] J. Korta, D. A. Clark, C. V. Gabel, L. Mahadevan, and A. D. Samuel. Mechanosensation and mechanical load modulate the locomotory gait of swimming *C. elegans*. *The Journal of Experimental Biology*, 210:2383–2389, 2007.
- [12] F. Leslie. The slow flow of a visco-elastic liquid past a sphere. *The Quarterly Journal of Mechanics and Applied Mathematics*, 14(1):36–48, 1961.

- [13] J. Lighthill. Flagellar hydrodynamics: The john von neumann lecture, 1975. *Society for Industrial and Applied Mathematics Review*, 18(2):161–230, 1976.
- [14] R. D. Maladen, Y. Ding, C. Li, and D. I. Goldman. Undulatory swimming in sand: Subsurface locomotion of the sandfish lizard. *Science*, 325:314–318, July 2009.
- [15] F. A. Morrison. *Understanding Rheology*. Oxford University Press, New york, New York, 2001.
- [16] D. Peters. Two-dimensional incompressible unsteady airfoil theory—an overview. *Journal of Fluids and Structures*, 24:295–312, 2008.
- [17] D. Peters, M. Hsieh, and M. Torrero. A state-space airloads theory for flexible airfoils. *Journal of the American Helicopter Society*, 51(4):329–342, 2007.
- [18] D. Peters, S. Karunamoorthy, and W. Cao. Two-dimensional thin airfoil. *The Journal of the Aircraft*, 32:313–322, 1995.
- [19] D. L. Riddle, T. Blumenthal, B. J. Meyer, and J. R. Rriess, editors. *C. elegans II*. Cold Spring Harbor Laboratory Press, Cold Spring Harbor, New York, 1997.
- [20] L. J. Rosenberger and M. W. Westneat. Functional morphology of undulatory pectoral fin locomotion in the stingray *Teaniura lymma* (chondrichthyes: Dasyatidae). *The Journal of Experimental Biology*, 202:3523–3539, 1999.
- [21] X. N. Shen and P. E. Arratia. Undulatory swimming in viscoelastic fluids. *Physical Review Letters*, 106:208101, 2011.
- [22] R. shine and S. Shetty. Moving in two worlds: aquatic and terrestrial locomotion in sea snakes (laticauda colubrina, laticaudidae). *Journal of Evolutionary Biology*, 14:338–346, 2001.
- [23] M. Silverman and M. Simon. Flagellar rotation and the mechanism of bacterial motility. *Letters to Nature*, 249:73–74, 1974.
- [24] J. Sznitman, X. Shen, R. Sznitman, and P. Arratia. Propulsive force measurements and flow behavior of undulatory swimmers at low reynolds number. *Physics of Fluids*, 22:121901, 2010.
- [25] G. Taylor. Analysis of the swimming of microscopic organisms. *Proceedings of the Royal Society of London*, 22(1099):447–461, 1951.
- [26] T. Theodorsen. General theory of aerodynamics instability and the mechanism of flutter. *NACA Report*, 496:413–433, 1934.

# Vita

Xialing Ulrich

**Date of Birth**      May 12, 1982

**Place of Birth**      Fujian, China

**Degrees**              B.S. Mechanical Engineering, Peking University, May 2003  
M.S. Mechanical Engineering, Peking University, May 2006  
D.Sc. Mechanical Engineering and Material Science, Washington University in Saint Louis, May 2012

**Publications**        Xialing Ulrich and David Peters, Sinusoidal locomotion of a flexible wing at high Reynolds numbers, *Journal of Fluids and Structures*, submitted (2012).

Xialing Ulrich, Eliot Fried, and Amy Shen, Crossover transition in flowing granular chains, *Physical Review E*, **80**, 030301 (2009).

May 2012

**Propulsion by Sinusoidal Locomotion, Ulrich, D.Sc. 2012**